NAVAL POSTGRADUATE SCHOOL
MONTEREY, CALIFORNIA

THESIS

EXPERIMENTAL STUDY OF INELASTIC STRESS CONCENTRATION AROUND A CIRCULAR NOTCH

by

Kenneth S. Long

March, 1996

Thesis Advisor: Young W. Kwon

Approved for public release; distribution is unlimited.

REPORT DOCUMENTATION PAGE

Form Approved OMB No. 0704-0188

1. AGENCY USE ONLY *(Leave blank)*	2. REPORT DATE March 1996	3. REPORT TYPE AND DATES COVERED Master's Thesis

4. TITLE AND SUBTITLE EXPERIMENTAL STUDY OF INELASTIC STRESS CONCENTRATION AROUND A CIRCULAR NOTCH

5. FUNDING NUMBERS

6. AUTHOR(S) Long, Kenneth S.

7. PERFORMING ORGANIZATION NAME(S) AND ADDRESS(ES)
Naval Postgraduate School
Monterey CA 93943-5000

8. PERFORMING ORGANIZATION REPORT NUMBER

9. SPONSORING/MONITORING AGENCY NAME(S) AND ADDRESS(ES)

10. SPONSORING/MONITORING AGENCY REPORT NUMBER

11. SUPPLEMENTARY NOTES The views expressed in this thesis are those of the author and do not reflect the official policy or position of the Department of Defense or the U.S. Government.

12a. DISTRIBUTION/AVAILABILITY STATEMENT
Approved for public release; distribution is unlimited.

12b. DISTRIBUTION CODE

13. ABSTRACT

Experiments were conducted to determine whether energy -density relations can be used to predict elastic-plastic stresses and strains near a circular notch for 7075-T6 aluminum alloys and ARALL 4 composites. The loading conditions were tension and four-point bending. Glinka and Neuber have developed relations that predict local inelastic strain response based on the stress-strain solution for small plastic zone sizes. It has been shown that these relations are appropriate for simple tension and in-plane bending, where stress and strain are uniform through the thickness. This study investigates the application of the Glinka and Neuber relations to samples where stress/strain is not constant though the thickness. Nonconstant stresses/strains are the result of out-of-plane bending and laminate characteristics.

14. SUBJECT TERMS Stress, strain, stress concentration factor, ARALL, composite, tension, bending, plasticity

15. NUMBER OF PAGES 90

16. PRICE CODE

17. SECURITY CLASSIFICATION OF REPORT	18. SECURITY CLASSIFICATION OF THIS PAGE	19. SECURITY CLASSIFICATION OF ABSTRACT	20. LIMITATION OF ABSTRACT
Unclassified	Unclassified	Unclassified	UL

NSN 7540-01-280-5500

Standard Form 298 (Rev. 2-89)
Prescribed by ANSI Std. 239-18 298-102

Approved for public release; distribution is unlimited.

EXPERIMENTAL STUDY OF INELASTIC STRESS CONCENTRATION AROUND A CIRCULAR NOTCH

Kenneth S. Long
Lieutenant, United States Navy
B.S. Petroleum Engineering, University of Texas at Austin, 1989

Submitted in partial fulfillment
of the requirements for the degree of

MASTER OF SCIENCE IN MECHANICAL ENGINEERING

from the

NAVAL POSTGRADUATE SCHOOL
March 1996

Author: _____
Kenneth S. Long

Approved by: _____
Young W. Kwon, Thesis Advisor

_____
Terry R. McNelley, Chairman
Department of Mechanical Engineering

ABSTRACT

Experiments were conducted to determine whether energy-density relations can be used to predict elastic-plastic stresses and strains near a circular notch for 7075-T6 aluminum alloys and ARALL 4 composites. The loading conditions were tension and four-point bending. Glinka and Neuber have developed relations that predict local inelastic strain response based on the stress-strain solution for small plastic zone sizes. It has been shown that these relations are appropriate for simple tension and in-plane bending, where stress and strain are uniform through the thickness. This study investigates the application of the Glinka and Neuber relations to samples where stress/strain is not constant though the thickness. Nonconstant stresses/strains are the result of out-of-plane bending and laminate characteristics.

TABLE OF CONTENTS

I. INTRODUCTION

An important aspect of fracture analysis and fatigue life prediction of a notched sample is the relationship between the load, the nominal elastic stress, and the elastic-plastic notch tip strain. Material failure is often initiated by the localized yielding from the stress concentration at a notch root. Because solutions for local stresses and strains in the inelastic region are difficult to obtain, researchers have attempted to solve for the inelastic stresses and strains based on simpler elastic solutions. A popular technique currently used to obtain accurate solutions is the finite element method (FEM). The drawbacks to this method are difficulties in using nonlinear elements and lengthy computational times, especially for a large number of cyclic loads. Approximate methods have been developed that generate good results in selected cases.

This study considers the energy-density method of approximating inelastic notch tip stresses and strains. The foundation of this method is that the energy density in the elastic range is nearly the same as the energy density in the inelastic range. Previous authors have applied this method to several types of steels and strain-hardening materials and to several types of notches (e.g., circular, elliptical, V, keyhole, etc.). They also considered tension, in-plane bending, and cyclic loading. The stress and strain in these tests were uniform through the sample thickness.

In this study, experimental testing was conducted on 7075-T6 aluminum alloy and aramid aluminum laminate (ARALL 4) samples with a stress concentration around a circular notch. By applying tension to the ARALL 4 sample and out-of-plane bending to both samples, a condition of nonconstant stress and strain through the thickness was created. To analyze these conditions, several assumptions were made:

- All samples were in a plane stress condition.
- For small scale localized plastic yielding around a notch, the inelastic energy density was the same as the elastic energy density.
- Sample loading was monotonic.
- A uniaxial stress state was considered at the vicinity of the notch tip because of the small local stress oriented transverse to loading direction.

The primary focus of this work is an experimental study to determine whether energy-density based approximation methods can be applied to 7075-T6 aluminum alloys for out-of-plane bending and ARALL 4 composites for both tension and out-of-plane bending. The material properties for each material will be verified and/or established for this study. For each loading type, the experimental setup will be described and the theory used to predict inelastic stresses/strains will precede the results of the tests.

II. LITERATURE SURVEY

A. IMPORTANT ADVANCES ON STRESSES AROUND CIRCULAR NOTCHES

In 1929, Howland [1] used a successive approximation method to solve for the stresses in a semi-infinite plate, with a circular hole mid-way between the parallel edges, under tension. He developed general formulas in an infinite series form that were used to plot the stress variation around the hole. Each term of the series was based on the ratio of hole diameter to plate width and constant coefficients were derived by Howland.

In 1939, Dumont [2] tested a large plate containing an open circular hole by subjecting the plate to uniform bending normal to the plane of the plate. He found that stress concentrations occurred at the edge of the hole. Further, stress became constant at a distance of 2.5 times the hole's diameter from the edge of the hole.

In 1952, Hill [3] stated that in practice the radius of curvature of the notch root must be two or three times the plate thickness if the theory of generalized plane stress is to be a satisfactory approximation.

In 1974, Peterson [4] published a book of stress concentration factors for numerous plate geometries. Related to this study was the plot of stress concentration factors for the transverse bending of a finite-width plate containing a circular hole. He did not plot the stress gradient ahead of a hole,

but rather the stress concentration factor at the edge of the hole for ratios of hole diameter to plate width from $\lambda = 0.0$ to 0.2.

In 1990, Prasad and Shuart [5] developed a closed form solution for the moment distribution around holes. Their analytical study considered symmetric composite laminates subjected to bending moments.

B. HISTORY OF ENERGY DENSITY METHOD

The most frequently used relation for predicting local elastic-plastic stresses and strains near notches was developed by Neuber [6] in 1961. More recent studies have shown that Neuber's rule can lead to considerable over-estimations of the elastic-plastic strains at the notch tip.

In 1964, Theocaris and Marketos [7] used a birefringent coating method complemented with the electrical analogy method to determine the distribution of principle stresses and strains around a circular notch. They considered AL57S, a strain-hardening aluminum alloy, for monotonic loading up to generalized plastic flow.

In 1968, Hutchinson [8] showed that the strain energy in the plastic zone ahead of a crack tip is the same as that calculated based on the linear elastic stress-strain analysis for material characterized by a bilinear stress-strain behavior. In other words, the energy density at the notch root does not change significantly if the localized plasticity is surrounded by predominately elastic material.

In 1981, Molski and Glinka [9] used Hutchinson's energy density theory

and made the assumption that the theory could be applied to notches and material exhibiting nonlinear stress-strain behavior. A uniaxial stress state was considered at the notch tip subject to cyclic loading.

In 1985, Glinka [10] applied the energy density method for a uniaxial stress state at the notch tip undergoing monotonic, nonproportional loading. Theoretical strain approximations were compared to experimental strains previously measured by Theocaris and Marketos [7]. Glinka compared inelastic notch tip strains for several notches and materials. This study uses the uniaxial stress state with monotonic loading and applies it to tension loading of an ARALL 4 composite and out-of-plane bending of 7075-T6 aluminum and ARALL 4 composite.

In Glinka's [11] second paper of 1985, he modified the strain energy density method by adding a factor C_p that accounts for the increase in plastic zone size due to local yielding. This factor becomes important when strains exceed 1.0 percent.

Also in 1985, Hoffmann and Seeger [12] developed a method of estimating elastic-plastic notch stresses and strains for a multiaxial stress state in the vicinity of the notch tip. This method applied to both monotonic and cyclic loading.

In 1988, Glinka, Ott and Nowack [13] used the equivalent strain energy density method to determine the elastic-plastic stresses and strains in notches under a plane strain condition. Results were compared with FEM solutions.

In 1992, Sharpe, Yang and Tregoning [14] conducted an in-depth review of the Neuber and Glinka relations for monotonic loading. They determined that in general, the Neuber method was best suited for a plane stress condition because it was conservative. The Glinka plane stress method provided an upper bound of stress. For large plastic deformation regions, the Glinka and Neuber methods bounded the experimental results.

In 1995, Lee, Chang and Wong [15] improved Hoffmann's and Seeger's method [12] for monotonic loading by taking a general approach. Multiaxial notch stresses and strains were estimated based on elastic notch stress solutions for in-phase or out-of-phase loading. The authors also reported that in general, the Glinka and Neuber methods underestimate the notch strain in the high yield deformation region and overestimate the local strain in the low plasticity zone.

III. MATERIAL PROPERTY VERIFICATION

This chapter describes the preliminary tests and results that were conducted on two types of material: 7075-T6 aluminum alloy and Aramid Aluminum Laminate (ARALL 4). Preliminary tests were required to verify and establish material properties for the material provided because that information was required for tests described in subsequent chapters.

A. 7075-T6 ALUMINUM ALLOY

1. Material

The aluminum alloy used in this study was cut from one sheet of 7075-T6 aluminum. This aluminum sheet metal was also identified by the Government Mill Form and Condition designation as QQ-A-250-12. Initial dimensions of the large sheet were: 54 in. (137.2 cm) x 46 in. (116.8 cm) x 0.125 in. (0.318 cm).

2. Experimental Apparatus

Tension tests were conducted on four test coupons to verify the 7075-T6 aluminum sheet metal material properties used in this study as compared with published 7075-T6 aluminum material properties. The test coupon design and the testing methods used were governed by American Society for Testing of Materials (ASTM) standard test methods [16]. Figure 1 shows the dimensions of the tension test coupons used for material verification. The methods listed in [16] were used to determine the material properties of yield

strength (offset=0.2%) and ultimate tensile strength. The testing methods used to determine Young's modulus and Poisson's ratio were listed in [17] and [18], respectively.

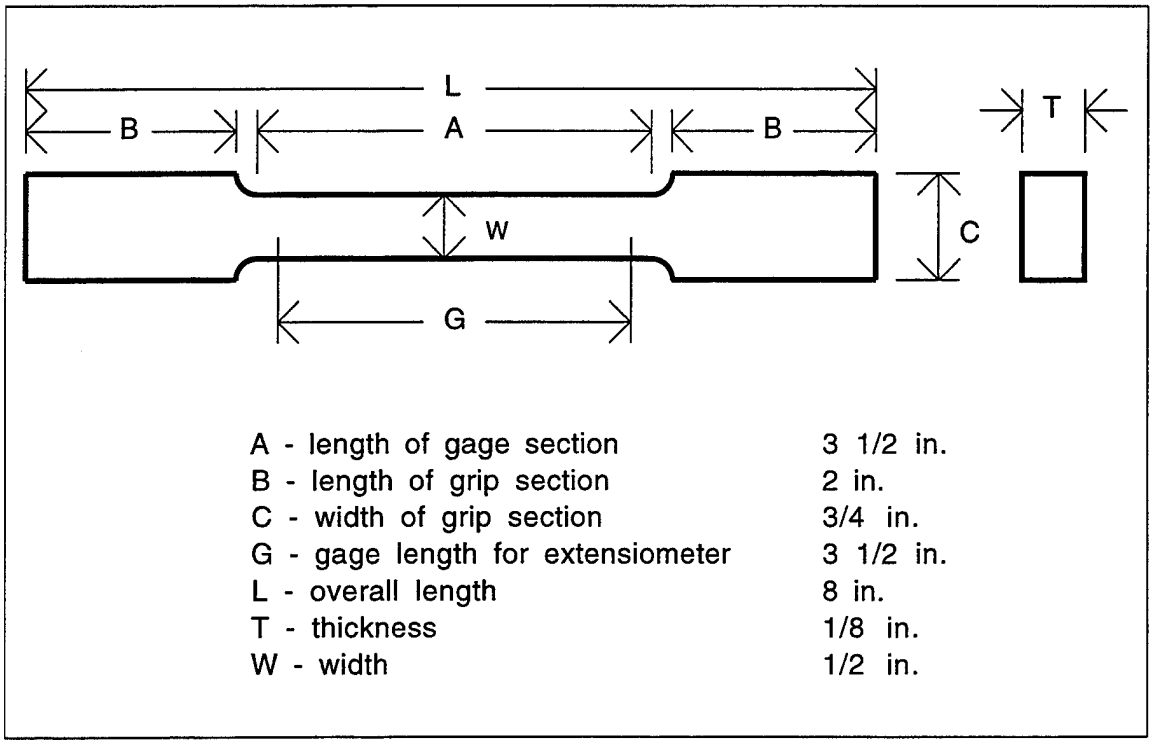

Figure 1. Tension Test Coupon Dimensions.

Test coupon width and thickness were measured using a Mitutoyo Digital Micrometer, accurate to 0.00005 in. (0.001 mm). The 90 degree strain gage rosettes used were Measurements Group Inc. type CEA-13-125UT, 120 ohm, gage factor 2.085 $\pm$ 0.5% (longitudinal) and 2.115 $\pm$ 0.5% (transverse). The Instron dynamic extensiometer used had a 3.5 in. (8.9 cm) gage length and a $\pm$ 0.2 in. (0.51 cm) range. The Instron Model 4507 tension/compression

test machine was used with a 200 KN load cell. Load and displacement data were obtained using the Instron Model 4500 data acquisition tower with the Instron series IX automated materials testing software, version 5.28. Strain gage readings were acquired through the Measurements Group P-3500 strain indicator/SB-100 switch and balance unit combination. These two units were used to acquire all the strain gage readings in following tests. The equipment set up used for this and subsequent tests is pictured in Figure 2. All data recorded from the tests was manually entered into MATLAB programs that generated the graphs presented in this study.

3. Results

Table 1 shows the comparison of the experimentally determined material properties with published material properties [19] for bare 7075-T6 aluminum alloy. The experimental results provided in Table 1 were based on data and calculations from three of the four test coupons. Three test coupons were cut in a longitudinal orientation from the aluminum sheet. Because transverse mechanical properties of many products, particularly tensile strengths and ductility in the short transverse direction, can be less than those in the longitudinal direction [20], one test coupon was cut from the sheet in a transverse direction to verify isotropic behavior in the aluminum sheet. A comparison of transverse and longitudinal material properties is listed in Table 2. Because transverse and longitudinal material properties were in good comparison, the aluminum sheet was considered isotropic.

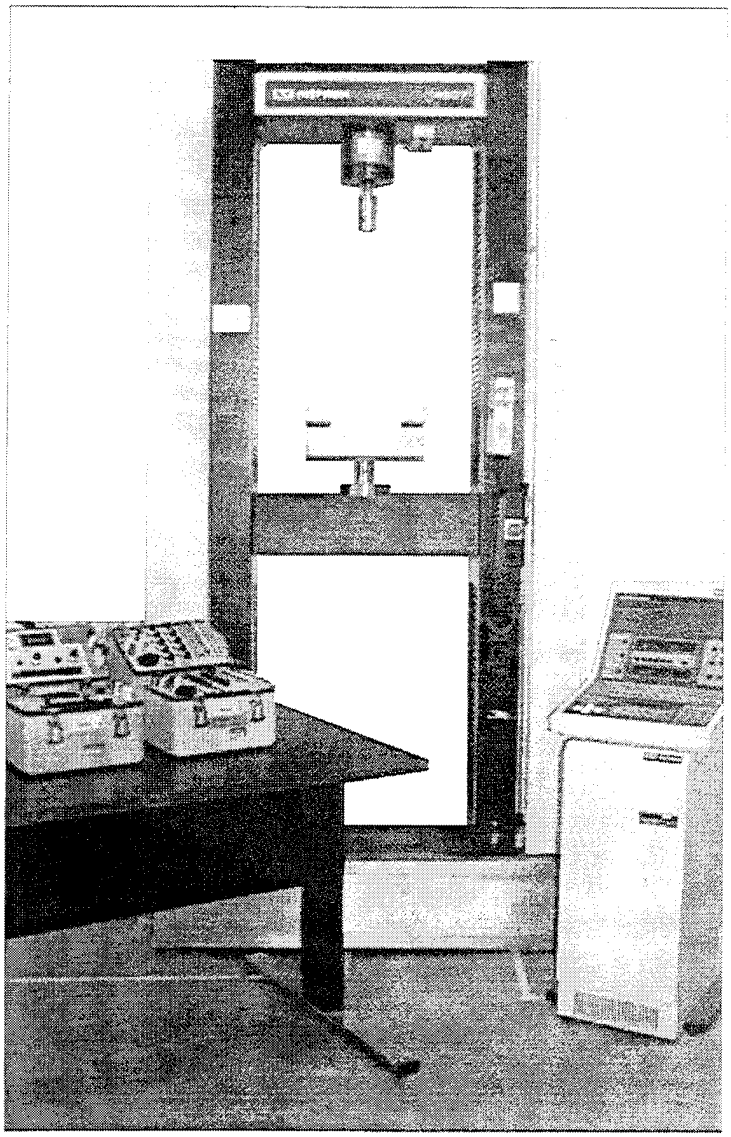

Figure 2. Test Equipment Setup.

	Experimental		Published		Percent Difference
	MPa	ksi	MPa	ksi	
Yield Strength (offset=0.2%)	505	73.3	503	73.0	0.4
Ultimate Tensile Strength	576	83.6	572	83.0	0.7
Young's Modulus	69,600	10,100	71,000	10,300	2.0
Poisson's Ratio	0.37		0.33		12.1

Table 1. Comparison of Experimental and Published Material Properties for 7075-T6 Aluminum Alloy.

	Sample 1 (transverse)	Sample 2 (longitudinal)	Sample 3 (longitudinal)	Sample 4 (longitudinal)
Yield Strength (offset=0.2%) (ksi)	69.9	73.2	73.4	73.3
Ultimate Tensile Strength (ksi)	83.2	83.5	83.7	83.7
Young's Modulus (ksi)	9,928	10,249	9,944	10,169
Poisson's Ratio	0.373	0.373	0.369	0.366

Table 2. Comparison of Transversly Oriented Sample 1 to Longitudinally Oriented Samples 2, 3, and 4.

a. Young's Modulus

For Young's modulus calculations, each test coupon was tension tested three times in the elastic range by cyclic loading, as per Reference 21. The modulus values calculated for each of the three runs were averaged, resulting in an average modulus value for that test coupon. The Young's modulus used in this study was the average modulus value of the three test coupons oriented in the longitudinal direction.

During the tensile tests, strain data was collected from two sources. One source was a strain gage rosette mounted on the geometric center of the test coupon. The other source was an extensiometer. Young's modulii were calculated using stress and both strain data sources. As before, modulus values calculated for each run were averaged to result in a modulus value for each test coupon. Averaging the longitudinally oriented test coupons' modulii based on extensiometer data resulted in Young's modulus of 10,269 ksi (70.6 GPa). The average longitudinal Young's modulus based on strain gage data was 10,121 ksi (69.6 GPa), a 1.5% difference. Reference 22 describes the standard method of recording strain data with the use of extensiometers. In order to prevent damage to the extensiometers by subjecting them to impact forces that occur at ultimate failure, they were removed just prior to sample failure. The only means of obtaining strain data up to ultimate failure was with the use of strain gages.

b. Poisson's Ratio

Reference 23 provided the standard method of experimentally determining Poisson's ratio using extensiometers. Since the use of strain gages and extensiometers produced similar results for Young's modulus, strain gage based data was also used for determining Poisson's ratio. The Instron data acquisition system and automated testing software computed the ultimate tensile strength. Yield strengths (0.2% offset) were taken from stress-percent elongation graphs.

c. Nonlinear Coefficients

A relation most often used for strain in the nonlinear region is the Ramberg-Osgood relation [24]

$$\varepsilon = \frac{\sigma}{E} + \left(\frac{\sigma}{K}\right)^{\frac{1}{n}} \tag{3.1}$$

where K is the strength coefficient and n is the strain-hardening index. K and n were experimentally determined from the results of the tension tests used for material property verification. For most metals, a log-log plot of true stress versus true plastic strain is modeled as a straight line [25]. However, the relationship often deviates from linearity at low strains and/or high strains [26]. The slope of the line is n and the intercept with the log true stress axis is K. Figure 3 shows the plot of log true stress versus log true plastic strain for sample 2. Similar plots were seen with samples 3 and 4. K and n values were calculated for samples 2, 3, and 4 and averaged. It is obvious that the data is

not linear throughout the plastic range, but it is satisfactory to calculate K and n for the strain range over which the log-log plot is linear. Therein lies the question of which region of the plot should be considered linear. Two cases of linear approximations were investigated. Case 1 considers the data points of log true plastic strain between -4 and -2.4. Case 2 considers the data points of log true plastic strain between -3.2 and -2.4. A least squares approximation of the data for both cases is shown in Figure 3. The results were K = 110.13 ksi, n = 0.0790 for case 1 and K = 114.88 ksi, n = 0.0946 for case 2. It will be shown later that the case 2 linear approximation for K and n will provide slightly better results. Thus, the average K and n values used in this study are 114.88 ksi and 0.0946, respectively.

4. Statistical Analysis

A statistical study was employed to determine the errors in the least squares method of approximation to Young's modulus calculations. Correlation coefficients (r) were calculated for each run and averaged for each test coupon. The test coupons' averaged coefficients were then averaged to obtain a single correlation coefficient. Correlation coefficients indicate the reliability of the curve fit to the data and a perfect curve fit has a coefficient equal to 1.0. The average correlation coefficient for longitudinally oriented stress-strain plots in the elastic region was 0.99979. When the data is basically linear, as was the case in these tensile tests, the correlation coefficient is not a very sensitive indicator of the precision of the data. McClintock found that

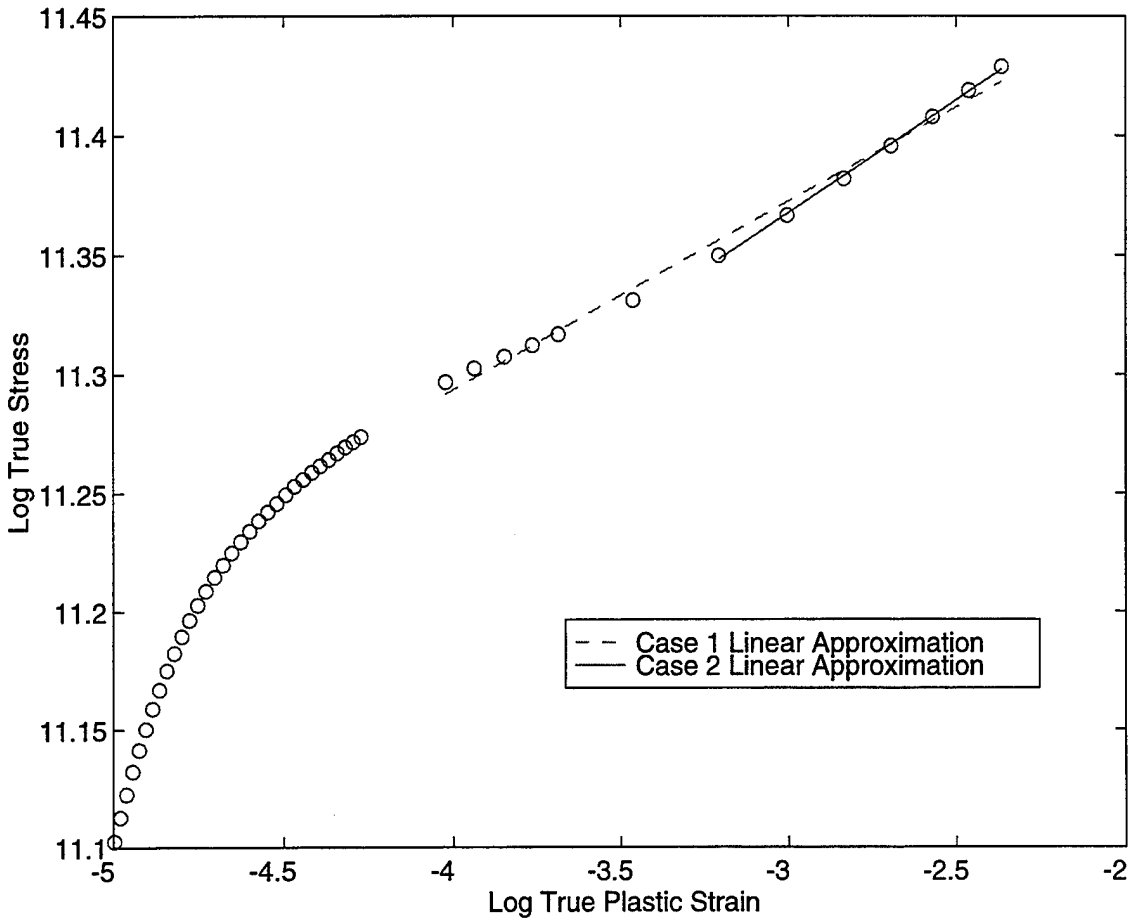

Figure 3. Log of True Plastic Stress-Strain Behavior for Sample 2. Strength Coefficient K and Strain Hardening Index n were determined using Case 2.

$(1-r^2)^{\frac{1}{2}}$ is a better indicator of the curve fit quality [27]. Here, $(1-r^2)^{\frac{1}{2}}$ = 0.0146. This value indicates that the vertical standard deviation of the data is only 1.46 percent of the total vertical variation caused by the straight-line relationship between stress and strain [28].

B. ARAMID ALUMINUM LAMINATE

1. Material

An aramid aluminum laminate (ARALL) has also been considered in this study. ARALL is classified as a polymer matrix composite material. The specific fiber-reinforced composite used was ARALL 4, which has a 5/4 configuration. There were five layers of 2024-T8 aluminum alloy and four layers of unidirectional and continuous Kevlar 49 aramid fibers. The laminate was symmetric and balanced with respect to the test direction. The 2024-T8 aluminum lamina were isotropic and all the aramid laminas were oriented in the same direction. Two sheets of the composite, measuring 12 inches by 12 inches each, were provided for testing.

2. Experimental Apparatus

Four samples were initially cut from the sheets provided. Two samples were machine finished to same dimensions as the 7075-T6 aluminum samples used for the material verification tensile tests (see Figure 1). One of these samples had the fibers oriented parallel to the loading direction and the other had the fibers oriented transverse to the loading direction. This design allowed for the calculation of longitudinal and

transverse modulii. The other two samples were machine finished to a rectangular shape of 1 in. (2.54 cm) by 9 in. (22.86 cm). These samples had fibers oriented only in the longitudinal direction and were used in flexural tests to determine the bending modulus.

The equipment used for the laminate material property tensile tests was the same as that used for the 7075-T6 aluminum material property tests. Figure 4 shows an ARALL sample undergoing a tension test. For the flexural tests, a four-point bending apparatus was constructed to determine bending modulus and it is shown in Figure 5. Four-point loading at the quarter points was the load configuration, which is a typical loading condition for high-modulus materials. The support span was 5 5/8 in. (143 mm) and the load span was 2 13/16 in. (71.5 mm). The sample length was 7 1/4 in. (188 mm) and laminate thickness was 3/32 in. (2.4 mm). Sample length was based on an ASTM recommended 60:1 span-to-thickness ratio for high-modulus composites. Deflection was measured using a Laboratory Devices Co. dial gage, accurate to 0.001 in. The strain gages used were Measurements Group Inc. type CEA-13-250UN, 350 ohm, gage factor 2.12 $\pm$ 0.5%. For both tensile and flexural tests, the Instron test machine was used in the manual load control mode to record load, strain and deflection data.

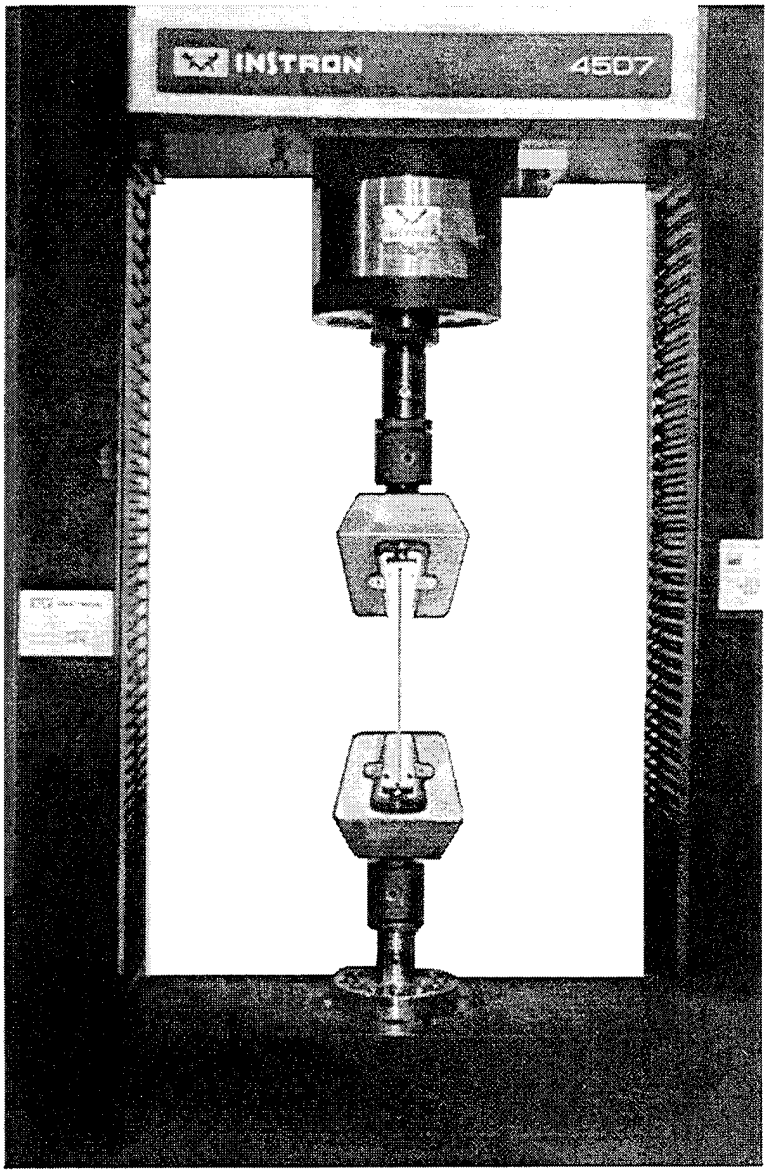

Figure 4. Tension Test of an ARALL 4 Sample.

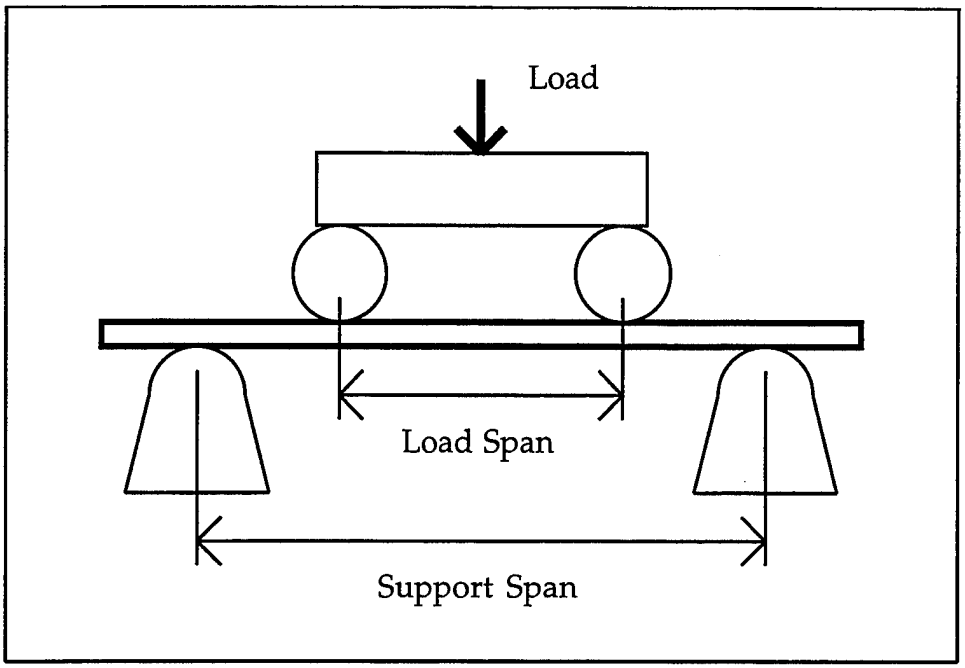

Figure 5. Four-Point Bending Apparatus for Flexural Tests.

3. Results

The reference used for the tensile test to determine Young's modulus and Poisson's ratio was ASTM 3039 [29] and the reference used for the flexural test to determine the bending modulus was ASTM 790 [30].

a. Young's Modulus

Two samples were tested to determine a smeared Young's modulus. This was the modulus for the laminate rather than a modulus for each of the different lamina. One sample was used to calculate E_1 (Young's modulus in the fiber direction) and the other was used to calculate E_2 (Young's modulus transverse to the fiber direction). Two strain gages were

placed on each sample. One gage was oriented in the fiber direction and the other gage was oriented transverse to the fiber direction. Although each sample was tested to ultimate failure, only data in the linear elastic range was used to calculate modulus values. For the sample with fibers oriented longitudinal to the loading direction, Figure 6 shows the stress-strain curves in the longitudinal and transverse directions. Figure 7 shows the stress-strain curves in the longitudinal and transverse directions for the case of fibers oriented transverse to the loading direction. Figure 8 shows the plot of stress versus strain for longitudinal and transverse directions in the linear elastic range. A MATLAB program was written to solve for the modulii in a least squares sense. The best fit approximation of the slope of the data in the elastic region for Figures 6 and 7 was the modulus value. For the longitudinal modulus, E_1 = 9,100 ksi (62.6 GPa) and for the transverse modulus, E_2 = 6,600 ksi (45.4 GPa). These modulii show that a sample with fibers oriented longitudinal to loading direction is stiffer than a sample with fibers oriented transverse to loading direction.

A comparison of the calculated E_1 value to published elastic modulii (tension) for 2024 aluminum and Kevlar 49 fibers is made. Because elastic modulii are dependent on laminate thickness and lamina orientation,a standard elastic modulus for the ARALL 4 material provided was not available. The published elastic modulus (tension) for 2024 aluminum is 10,500 ksi (72.4 GPa) [31] and for Kevlar 49 fibers is 18,100 ksi (125

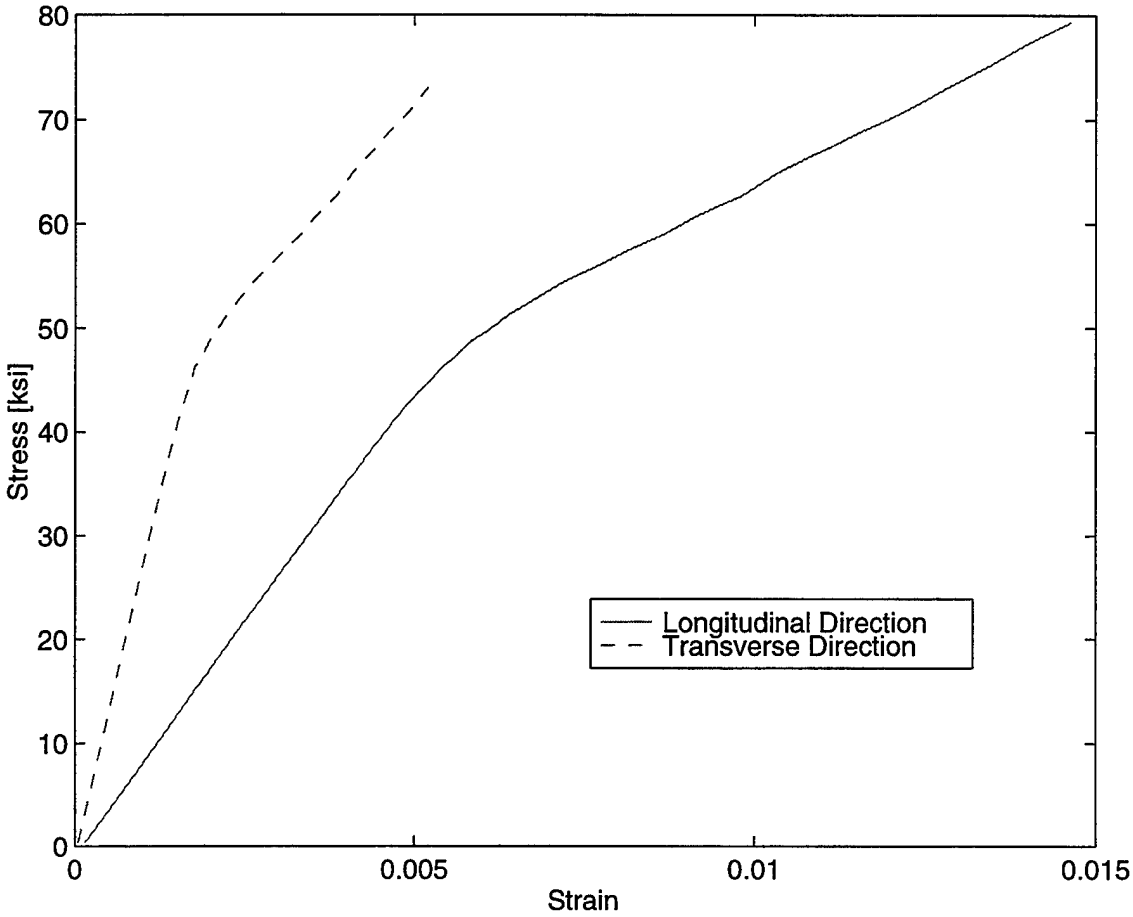

Figure 6. Stress-Strain Behavior in Longitudinal and Transverse Directions for Fibers Oriented Longitudinal to Loading Direction.

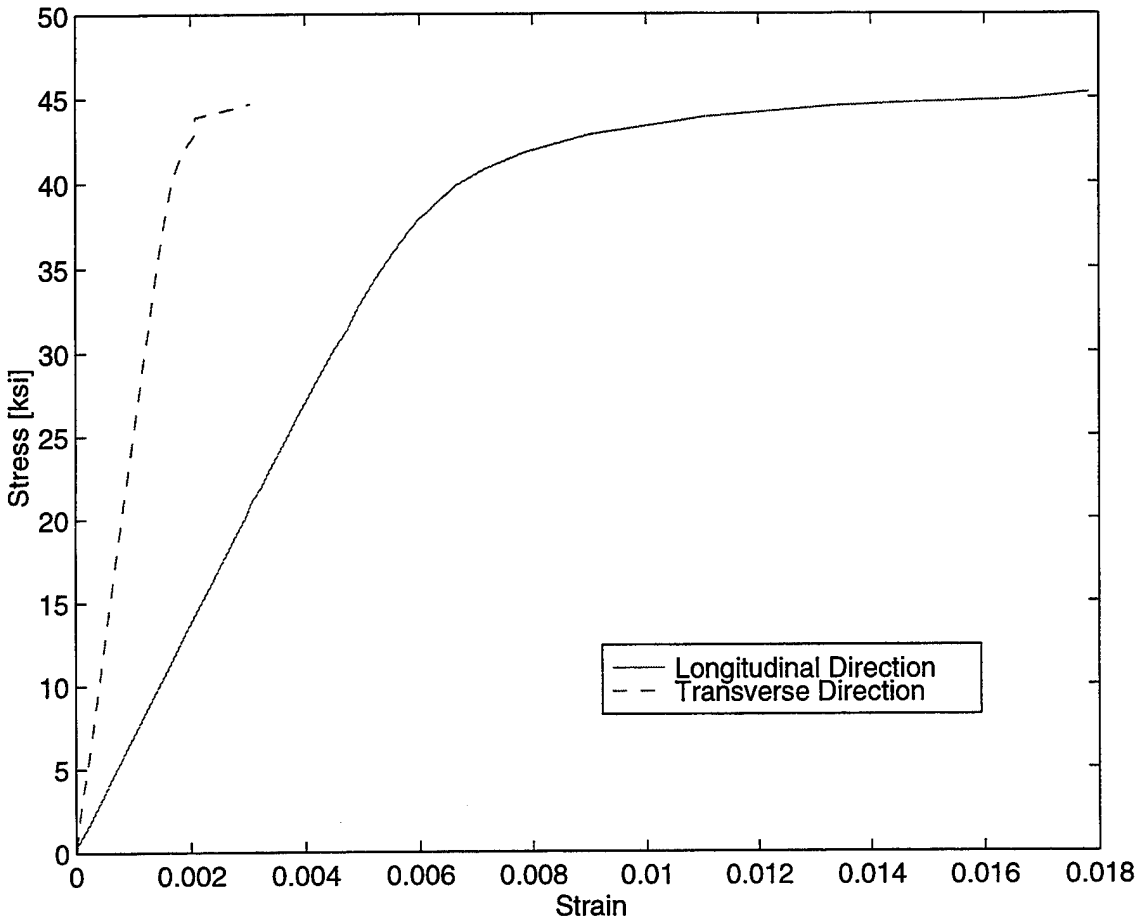

Figure 7. Stress-Strain Behavior in Longitudinal and Transverse Directions for Fibers Oriented Transverse to Loading Direcion.

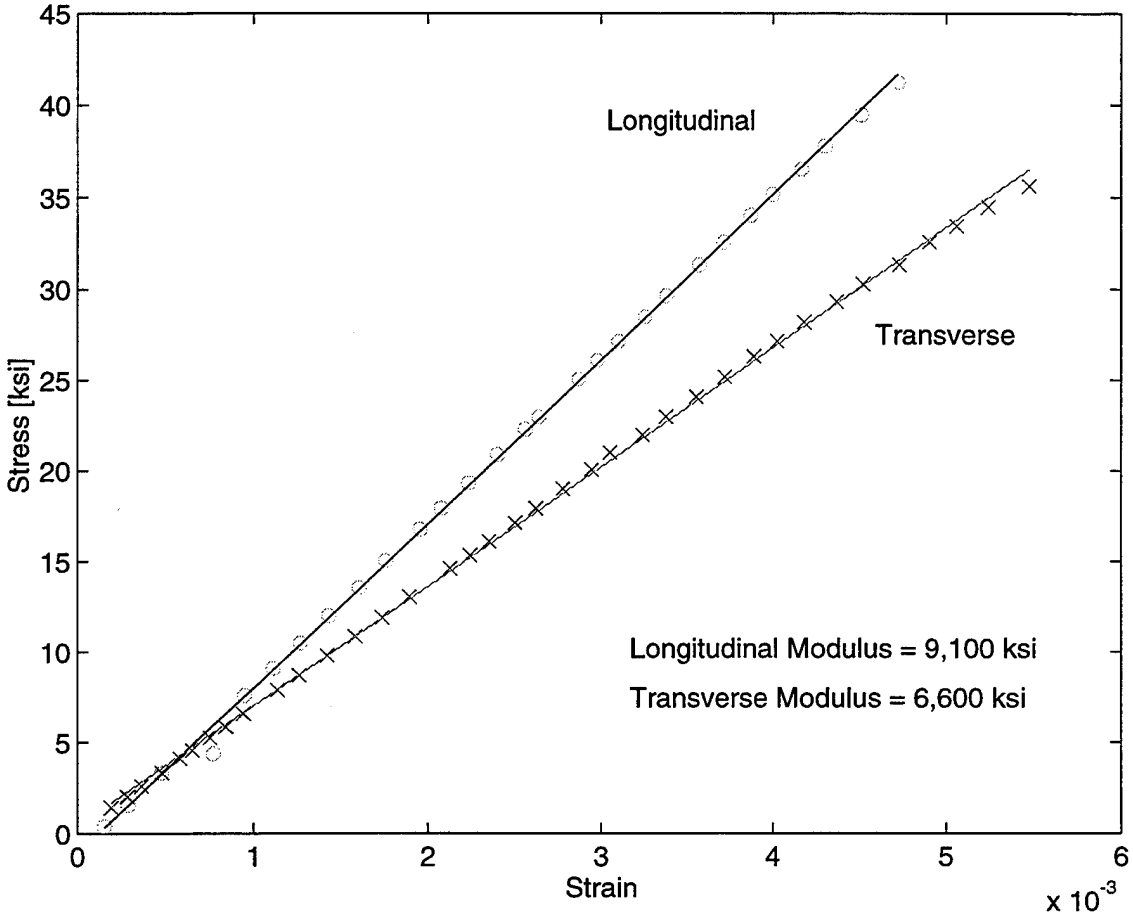

Figure 8. Longitudinal and Transverse Modulii in the Elastic Range.

GPa) [32]. Although the elastic modulus for Kevlar 49 is high, the lamina did not consist of a 100 percent volume fraction of Kevlar 49 fibers. These lamina contained an undetermined amount of resin, interface bonding material, and volume fraction of Kevlar 49 fibers much less than 100 percent. The low volume fraction of Kevlar 49 fibers effectively lowers the laminar elastic modulus to a percentage equal to the volume fraction. Thus, laminate elastic modulus values greatly depend on the volume fraction of the fibers within the lamina. It follows that E_1 = 9,100 ksi (62.6 GPa) is a reasonable laminate elastic modulus.

b. Bending Modulus

An alternative approach to tensile testing of unidirectional polymeric-matrix composites involves the bending of beam-type samples [33]. The flexural test method was used to determine a smeared bending modulus for the overall laminate vice individual 2024 aluminum or aramid aluminum lamina modulii.

Two samples were also used in flexural tests to determine the bending modulus, E_B. The purpose of using two samples was to achieve repeatability of the data. Since the results for each sample were nearly identical, only one sample's data will be presented. Figure 9 shows the plot of load versus deflection in the elastic range. For the test, E_B = 11,200 ksi (77.0 GPa). The bending modulus was calculated using

$$E_B = \frac{0.17L^3 m}{bt^3} \tag{3.2}$$

where L = length of support span [in. (mm)], b = with of beam [in. (mm)], t = thickness of beam [in. (mm)], and m = slope of load-deflection curve in elastic range [lbf/in. (N/mm)].

For laminate composites, the tensile modulus and bending modulus are expected to be slightly different. With highly anisotropic laminates, the bending modulus is strongly dependent on the lamina-stacking sequence [34]. A tensile modulus is not stacking-sequence dependent. In the flexural test conducted, the bending modulus E_B was 19 percent higher than the longitudinal modulus E_1. This can be explained by the different stiffnesses of the lamina. The 2024 aluminum lamina are stiffer than the aramid fiber lamina. The outermost lamina of the composite were the 2024 aluminum lamina. The stiffer outermost lamina results in higher bending stiffness but has no effect on the tensile stiffness.

c. Poisson's Ratio

The strain data taken from each sample used in the Young's modulus section was used to determine Poisson's ratio. Two Poisson's ratios were calculated. ν_{12} corresponds to the sample with fibers oriented longitudinally to the loading direction, while ν_{21} is for the sample with fibers oriented transverse to the loading direction. Figure 10 shows Poisson's ratio,

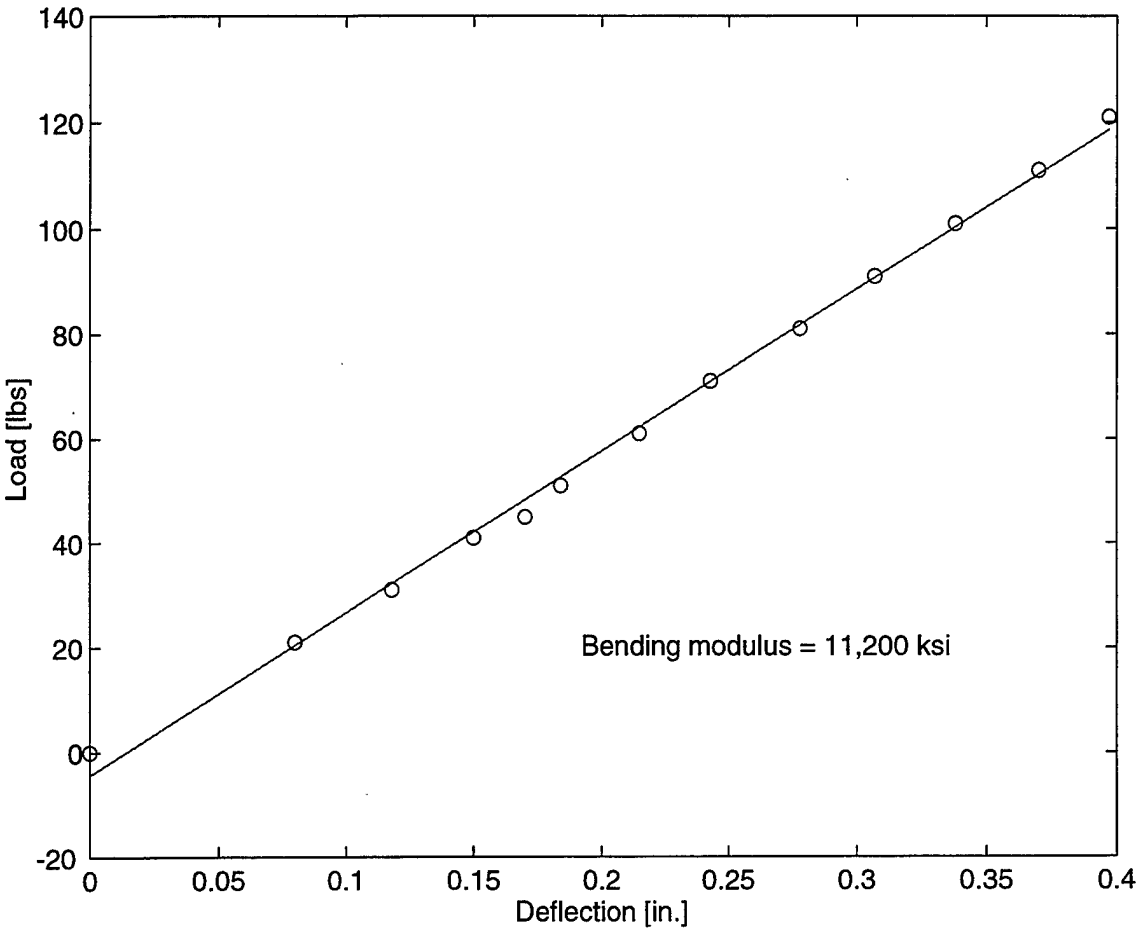

Figure 9. Load-Deflection Response for Flexural Test in Elastic Range used to Determine Bending Modulus.

ν_{12}, plotted versus load in the elastic region. The average value is drawn bythe horizontal line and calculated by

$$\nu_{avg} = \frac{\sum_{i=1}^{n} \frac{\varepsilon_{ti}}{\varepsilon_{li}}}{n} \tag{3.3}$$

where ε_{li} is the longitudinal strain, ε_{ti} is the transverse strain, and n is the total number of data points in the elastic region. This calculation was used to find $\nu_{12} = 0.323$. Reference 31 reports Poisson's ratio as 0.33 for 2024 aluminum. This compares nicely with the calculations for ν_{12}. Since the laminae containing longitudinally oriented Kevlar 49 fibers have almost no transverse stiffness, the laminate Poisson's ratio was essentially due to the effects of the 2024 aluminum lamina.

The relation

$$\frac{\nu_{12}}{E_1} = \frac{\nu_{21}}{E_2} \tag{3.4}$$

can be used to predict ν_{21}, since the other values are known. The calculation yields $\nu_{21} = 0.234$. For comparison, the plot of experimentally determined Poisson's ratio, ν_{21}, versus load in the elastic region is shown in Figure 11. Averaging the ratios results in $\nu_{21} = 0.270$, which is 15 percent higher than the

predicted value. This difference can be attributed several factors. One factor is that the experimental precision used to determine Young's modulus is related to gage factor errors and load readout errors. Another factor is that the plot of ν_{21} values in Figure 11 shows a wide range of data point scatter. However, the predicted ν_{21} value does fall within the range of data point scatter. The factors combine to give a slightly higher ν_{21} than expected. As expected, Figures 10 and 11 also show that Poisson's ratio is higher for fibers oriented in the loading direction than in the transverse direction.

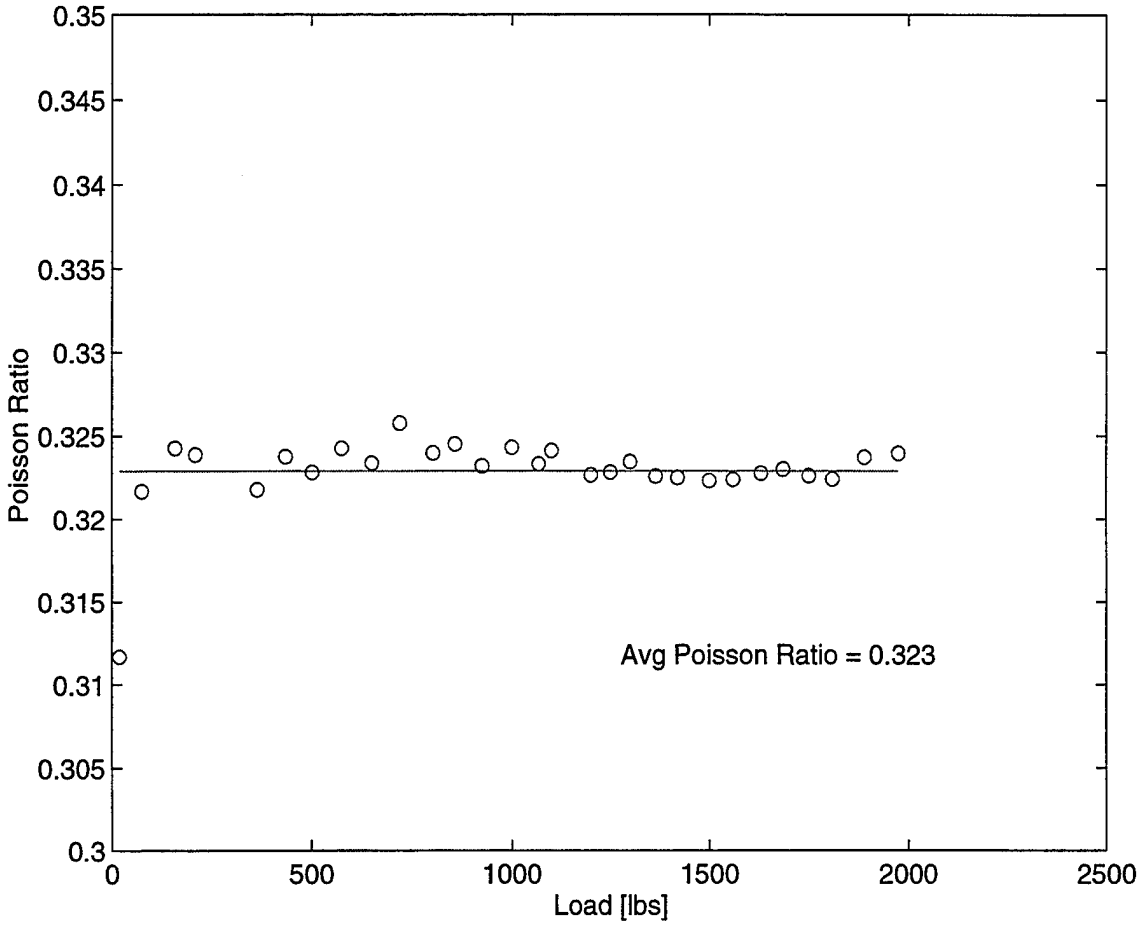

Figure 10. Poisson's Ratio in the Elastic Range for Fibers Oriented Longitudinal to Loading Direction.

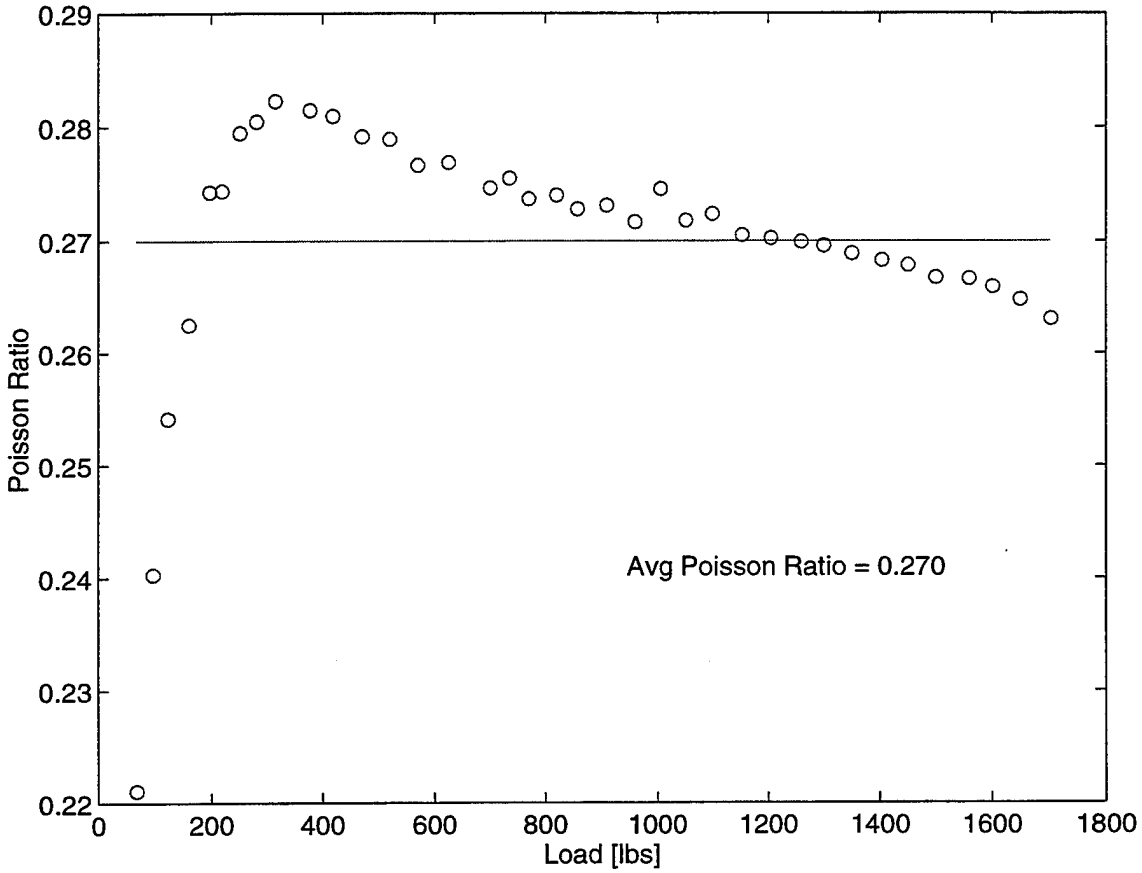

Figure 11. Poisson's Ratio in the Elastic Range for Fibers Oriented Transverse to Loading Direction.

IV. TENSION TEST

Tension tests on circular notched samples were conducted for both the 7075-T6 aluminum and the aramid aluminum laminate samples. The purpose of the tests on the 7075-T6 aluminum was to verify Glinka's previous work in Reference 10 and to validate the equipment used in this study. Tension testing on the ARALL 4 was done to determine if the energy-density method of calculating inelastic stress-strain near a circular notch, under plane stress conditions, could be applied to an ARALL 4 composite. This chapter discusses the equipment apparatus used for tension testing, the theory of the energy-density method based on two different equations, the method of computations for each material, and the results of the comparison of Glinka's and Neuber's theoretical inelastic stress-strain approximations to experimental stresses and strains. Test results indicated that the Glinka and Neuber methods worked as well as expected for the 7075-T6 aluminum sample but not for the ARALL 4 sample. Good theoretical inelastic strain predictions can be made using modified Glinka and modified Neuber methods.

A. EXPERIMENTAL APPARATUS

Figure 12 shows the geometry and dimensions of the circular notched samples used for the tension tests. The length of the 7075-T6 aluminum sample was 15 in. and the length of the ARALL 4 sample was 12 in. Both

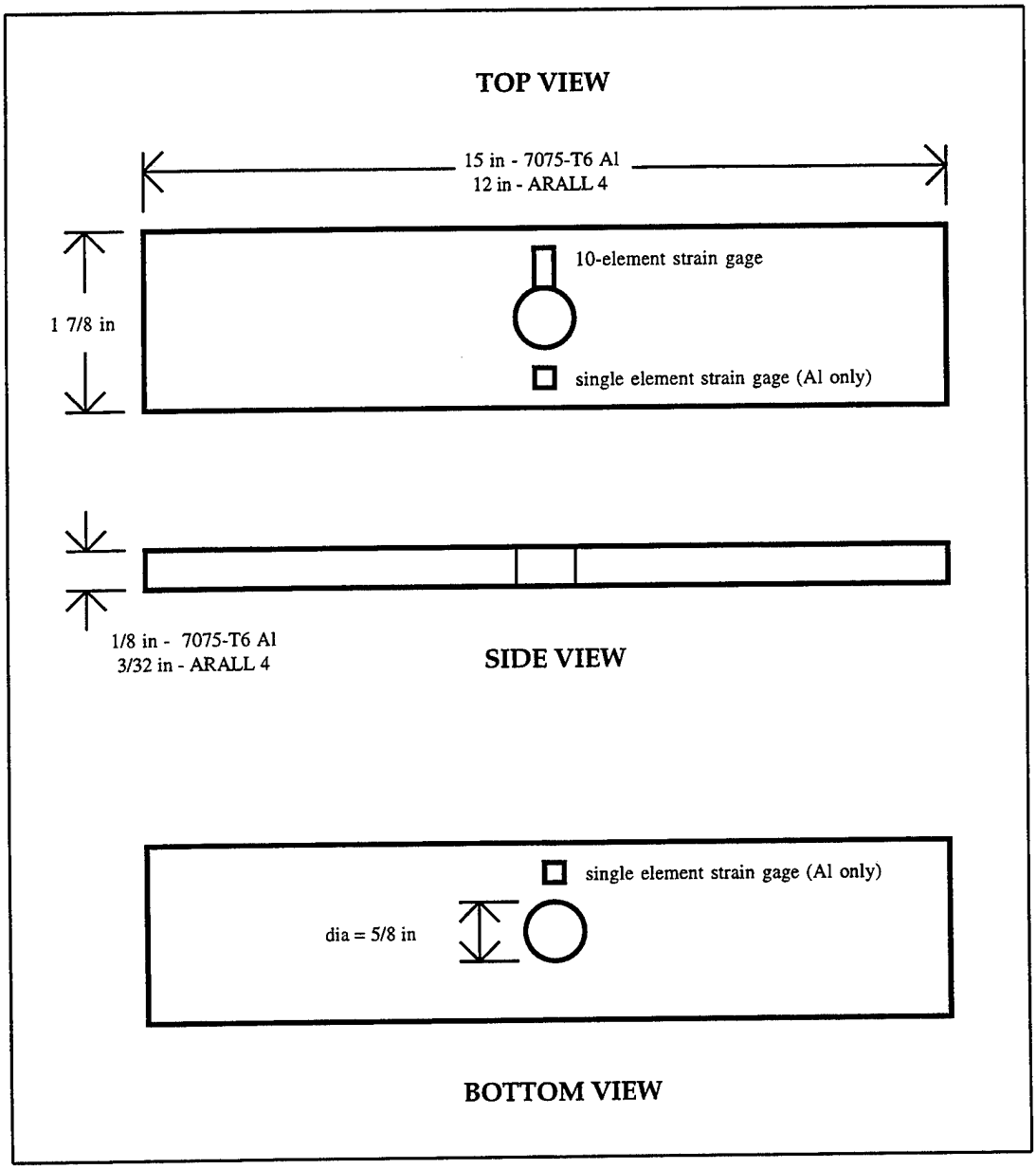

Figure 12. Circular Notched Sample Dimensions and Strain Gage Locations.

sample types had machine finished edges. The circular notch was milled through in the 7075-T6 aluminum sample and drilled through in the ARALL sample. The circular notch was located in the geometric center of the sample. Also shown in Figure 12 is the location and orientation of the strain gages. The 10-element strain gages used were Measurements Group Inc. type CEA-09-020PF, 120 ohm, gage factor 2.00 $\pm$ 3.0%. The single element strain gages used were Measurements Group Inc. type CEA-13-032UW, 120 ohm, gage factor 2.11 $\pm$ 1.0%. The two single element strain gages were positioned back-to-back only on the 7075-T6 aluminum sample. Having the two single gages positioned back-to-back and midway between the outer edge of the hole and edge of the sample permitted the comparison of strains on both sides of the sample. Greater strains on one side of the sample would indicate the presence of bending stresses caused by misaligned sample gripping. Tension tests were conducted on the Material Test System (MTS) Model 810 tension/compression test machine. The load cell cartridge was rated at 25 kips and the maximum deflection cartridge was rated at 1 inch. The MTS test machine was selected for testing because the grip width was 2 in., which was wide enough to extend across the entire width of the circular notched samples. A circular notched sample undergoing a tension test is pictured in Figure 13. For the 7075-T6 aluminum sample, the length of the sample gripped by the MTS machine was 2 in. on each end. The ARALL 4 sample gripped length was 1.25 in. on each end. The MTS machine was manually

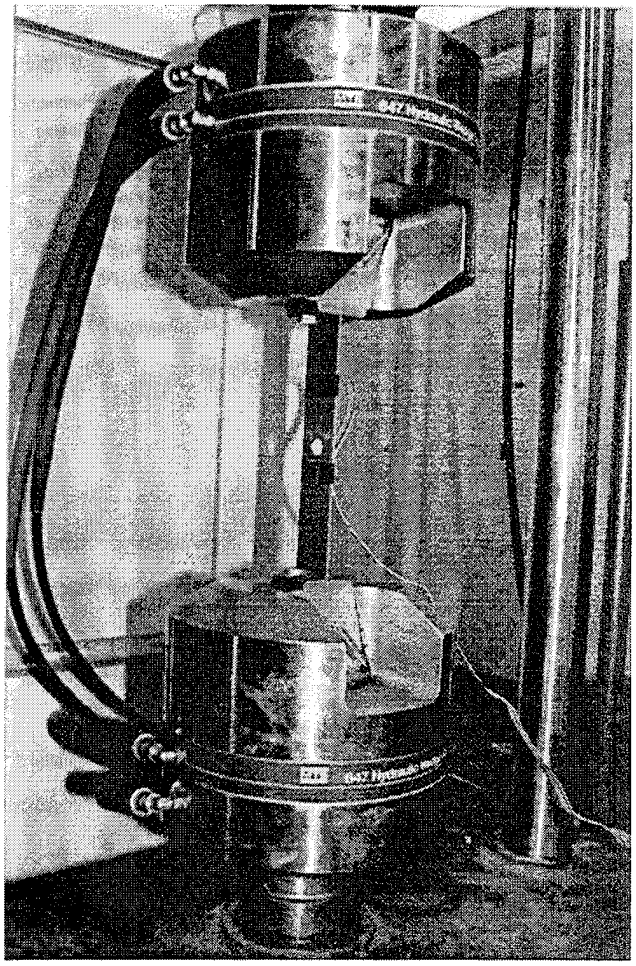

Figure 13. Tension Test of a Circular Notched Sample.

load controlled. Using a 10,000 sec/in. loading speed, the loading was periodically paused to allow recording of load and strain data. Samples were loaded to ultimate failure.

B. THEORY OF ENERGY-DENSITY METHOD

1. Based on the Ramberg-Osgood Relation

In Reference 10, Glinka described the energy-density method for calculating inelastic stresses-strains near notches. To assist the reader, the energy-density method of calculating inelastic stress-strain near a circular notch under plane stress conditions is presented below.

To calculate the energy density, a stress-strain relation must be applied. Well known and often used, the Ramberg-Osgood relation is

$$\varepsilon = \varepsilon_e + \varepsilon_p = \frac{\sigma}{E} + \left(\frac{\sigma}{K}\right)^{\frac{1}{n}}. \tag{4.1}$$

The strain energy density distribution ahead of a notch tip, W_s, can be calculated as

$$W_s = \int_0^{e_{ij}} S_{ij}\, de_{ij} \tag{4.2}$$

where S_{ij} is the local elastic stress tensor and e_{ij} is the local elastic strain tensor. For localized small-scale plastic yielding, the energy density in the plastic zone is nearly equal to that in the elastic zone. Thus, the energy density W_σ in the plastic zone is equal to that calculated on the basis of an elastic solution

$$W_s = W_\sigma \text{ or } \int_0^{e_{ij}} S_{ij}\,de_{ij} = \int_0^{\varepsilon_{ij}} \sigma_{ij}\,d\varepsilon_{ij} \tag{4.3}$$

where σ_{ij} is the local inelastic-plastic stress tensor and ε_{ij} is the local elastic-plastic strain tensor.

The elastic stress at the notch tip is

$$S_y = K_t \cdot S_n \tag{4.4}$$

where S_y is the local elastic stress component in the y direction, K_t is the stress concentration factor, and S_n is the nominal stress. For uniaxial stress at the notch tip, equation (4.3) can be written in the form

$$\frac{(K_t \cdot S_n)^2}{2E} = \frac{S_y^2}{2E}. \tag{4.5}$$

This states that elastic strain energy density W_s at the notch tip is equal to the product of the strain energy density W_{sn} due to the nominal stress S_n and the square of the stress concentration factor K_t

$$K_t^2 W_{sn} = W_\sigma. \tag{4.6}$$

With localized yielding at the notch tip, the energy density should be calculated with respect to the nonlinear stress-strain relation (4.1), then equation (4.6) takes the form

$$K_t^2 \frac{S_n^2}{2E} = \frac{\sigma_y^2}{2E} + \frac{\sigma_y}{n+1}\left(\frac{\sigma_y}{K}\right)^{\frac{1}{n}}. \tag{4.7}$$

When the nominal stress S_n has exceeded the proportional limit, equation

(4.6) takes the form

$$K_t^2[\frac{S_n^2}{2E} + \frac{S_n}{n+1}(\frac{S_n}{K})^{\frac{1}{n}}] = \frac{\sigma_y^2}{2E} + \frac{\sigma_y}{n+1}(\frac{\sigma_y}{K})^{\frac{1}{n}}. \quad (4.8)$$

Equations (4.7) and (4.8) enable one to calculate the inelastic stress σ_y and strain ε_y at the notch tip for given nominal stress S_n and stress concentration factor K_t. S_n is easily calculated from

$$S_n = \frac{P}{A_{min}} \quad (4.9)$$

where P is the tensile load and A_{min} is the minimum cross-sectional area of the sample.

Neuber [6] derived a relation to calculate local inelastic strain ε_N and stress σ_N. In the elastic region, the energy-density method and Neuber's rule are the same. However, in the inelastic region, Neuber's rule takes the form

$$K_t^2[\frac{S_n^2}{2E} + \frac{S_n}{2}(\frac{S_n}{K})^{\frac{1}{n}}] = \frac{\sigma_N^2}{2E} + \frac{\sigma_N}{2}(\frac{\sigma_N}{K})^{\frac{1}{n}}. \quad (4.10)$$

but the right hand side does not represent energy density. σ_N is the Neuber determined inelastic stress. The difference between Neuber's rule and Glinka's energy-density relation (4.8) is the $\frac{1}{1+n}$ before the second term in each side of (4.8) is replaced by a $\frac{1}{2}$ in (4.10).

2. Based on the Bilinear Relation

It will be shown later in this chapter that the predicted theoretical inelastic notch strains for the ARALL 4 composite are unsatisfactory when the Glinka and Neuber methods are used. The Glinka and Neuber equations can be modified to account for the bilinear stress-strain behavior of the ARALL 4 composite.

In the upper linear region of the bilinear stress-strain diagram, (4.7) becomes

$$K_t^2 \frac{S_n^2}{2E} = \frac{\sigma_1^2}{2E} + \frac{(\sigma_y^2 - \sigma_1^2)}{2E_t}, \quad \text{for } (\sigma_y < \sigma_1) \tag{4.11}$$

where E_t is the modulus in the upper linear region [ksi] and σ_1 is the stress at the intersection of each linear region [ksi]. Theoretical inelastic notch strains for the modified Glinka method are approximated using

$$\varepsilon = \frac{\sigma_y - \sigma_1}{E_t} + \varepsilon_1 \tag{4.12}$$

where ε_1 is the strain at the intersection of each linear region.

Neuber's method may be modified to account for the bilinear stress-strain behavior, such that

$$K_t^2 \frac{S_n^2}{2E} = \frac{\sigma_N}{2}\left(\frac{\sigma_N - \sigma_1}{E_t} + \frac{\sigma_1}{E}\right) \tag{4.13}$$

where σ_N represents the stress from Neuber's method [ksi]. Theoretical

inelastic notch strains for the modified Neuber's method are also found using (4.12).

C. METHOD OF COMPUTATIONS

To compare experimental stress-strain with theoretical stress-strain determined by the energy-density method, the experimental data was entered into a MATLAB program. The different material types required different equations to solve for inelastic notch strains.

1. 7075-T6 Aluminum Alloy

For nominal stresses lower than the yield stress, theoretical elastic strains were calculated using Hooke's Law. Equations (4.8) and (4.10) were used to compute Glinka's and Neuber's theoretical inelastic stresses based on the nominal stresses calculated in (4.9). Because (4.8) and (4.10) are nonlinear, the bisection numerical technique was employed to solve for the theoretical inelastic stresses. Theoretical inelastic strains were calculated by substituting the theoretical inelastic stresses from (4.8) and (4.10) into (4.1).

2. ARALL 4 Composite

In the elastic region, strains were calculated using Hooke's Law and Glinka's equation (4.7). Inelastic strains were calculated using Glinka's equation (4.10). These equations produced unsatisfactory results. Better results were obtained when Glinka's and Neuber's methods were modified in (4.11) and (4.13). Inelastic stresses were calculated from (4.11) and (4.13) and substituted into (4.12) to obtain inelastic strains.

D. RESULTS

1. 7075-T6 Aluminum Alloy

a. Theoretical Circular Notch Strain

Figure 14 shows that the Ramberg-Osgood relation produces a good stress-strain approximation to experimental data for 7075-T6 aluminum. However, the decision as to which data points to consider to determine the strength coefficient K and strain hardening index n can affect the results. Figure 15 shows the comparison of Glinka's theoretical notch strain to experimental notch strain for tensile loading. The experimentally determined stress-strain curve is added to Figure 15 for reference. Two theoretical approximations, cases 1 and 2, are shown. In Case 1, K = 110.13 ksi and n = 0.0790. In Case 2, K = 114.88 ksi and n = 0.0946. As previously mentioned in Chapter III and now apparent, case 2 K and n material property values provide a closer approximation to experimental results. During elastic behavior, the experimental, theoretical, and stress-strain curves are the same. The deviation of the experimental and theoretical curves from the stress-strain curve occurs at the beginning of inelastic behavior. In the inelastic range, the results confirm Glinka's results [10] in that, "The difference between calculated and measured notch strains were smaller than 10 percent ...". For the 7075-T6 aluminum sample, the maximum calculated and measured strain difference was 11.8 percent in the inelastic region. This experiment confirmed the Lee et al. [15] claim that Glinka's rule

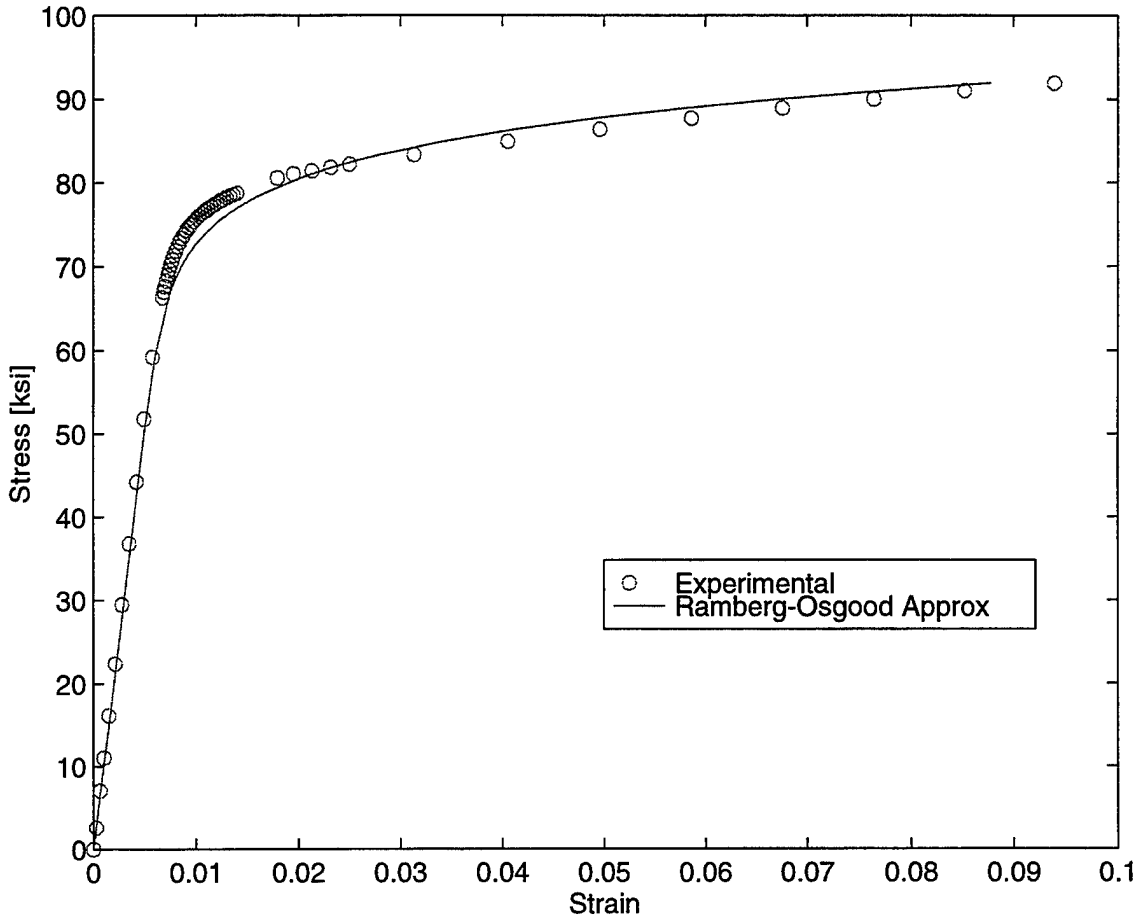

Figure 14. Ramberg-Osgood Stress-Strain Approximation to Experimental Data for 7075-T6 Aluminum Alloy.

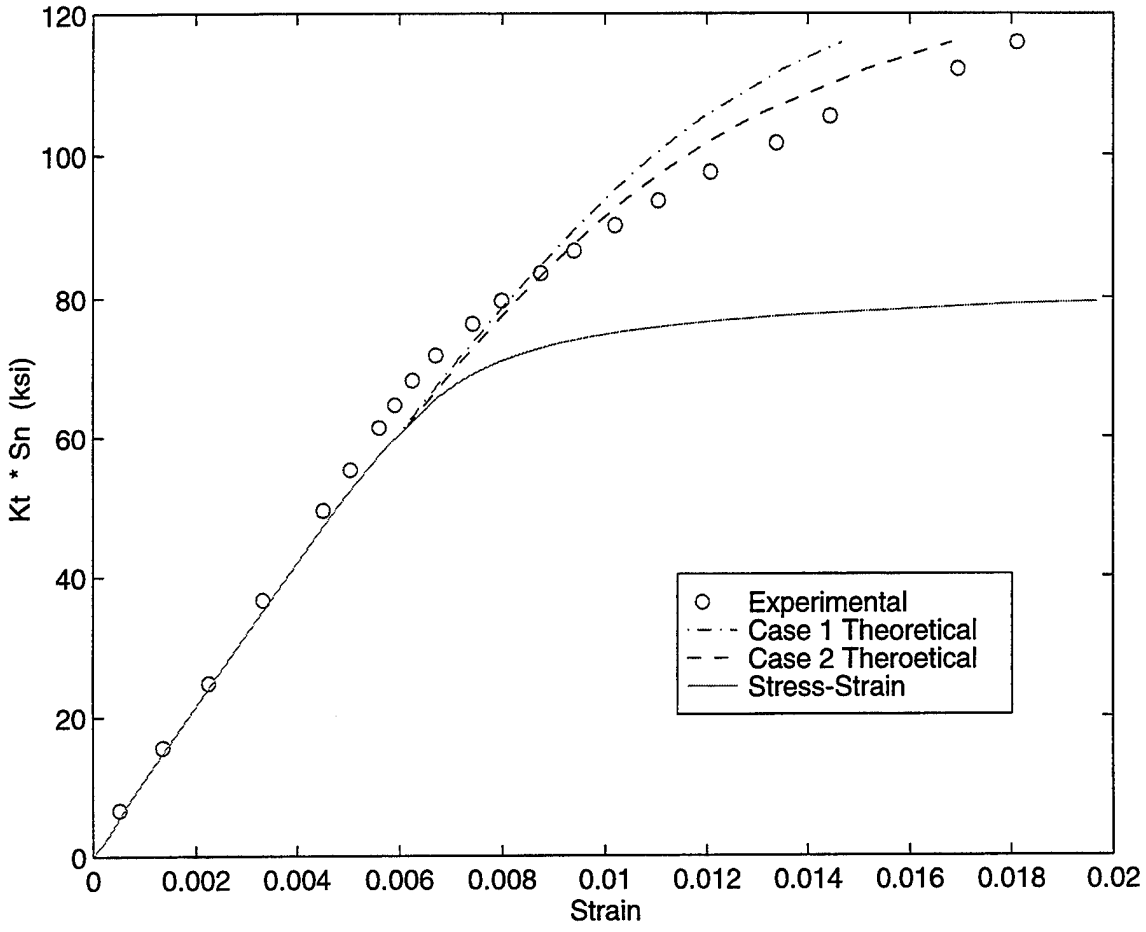

Figure 15. Comparison of Theoretical and Experimental Circular Notch Strains in 7075-T6 Aluminum Alloy for Two Different Cases of K and n Values.

underestimates the notch strain in the high yield deformation region and overestimates the local strain in the low plasticity zone.

Figure 16 shows the comparison of Glinka and Neuber methods for determining theoretical circular notch strain in 7075-T6 aluminum. As Glinka [10] indicated, Neuber's rule underestimates notch strain. However, Sharpe et al. [14] reports that the Neuber rule is the best single model for predicting notch strains in a plane stress condition. This is because the Neuber rule is more conservative than the Glinka rule. For large plastic deformation regions, the Glinka plane stress model gives an upper bound of strain. The sample reached ultimate failure at a tensile load of 13,270 lbs; the corresponding nominal stress was 85.0 ksi.

b. Stress Concentration Factors

The plot of theoretical and experimental circular notch strains proved to be very sensitive to the selection of the elastic stress concentration factor K_t. The elastic stress concentration factor gradient ahead of the notch was calculated using Howland's method of coefficients [1]. The ratio of hole diameter to plate width was $\lambda = 0.334$. Howland only calculated coefficients for the ratios of $\lambda = 0.1, 0.2, 0.3, 0.4$ and 0.5. Thus, the coefficients used in this study had to be interpolated from Howland's table of coefficients. The stress concentration factor gradient away from the notch is shown in Figure 17. The gradient is steepest near the notch and decreases away from the notch.

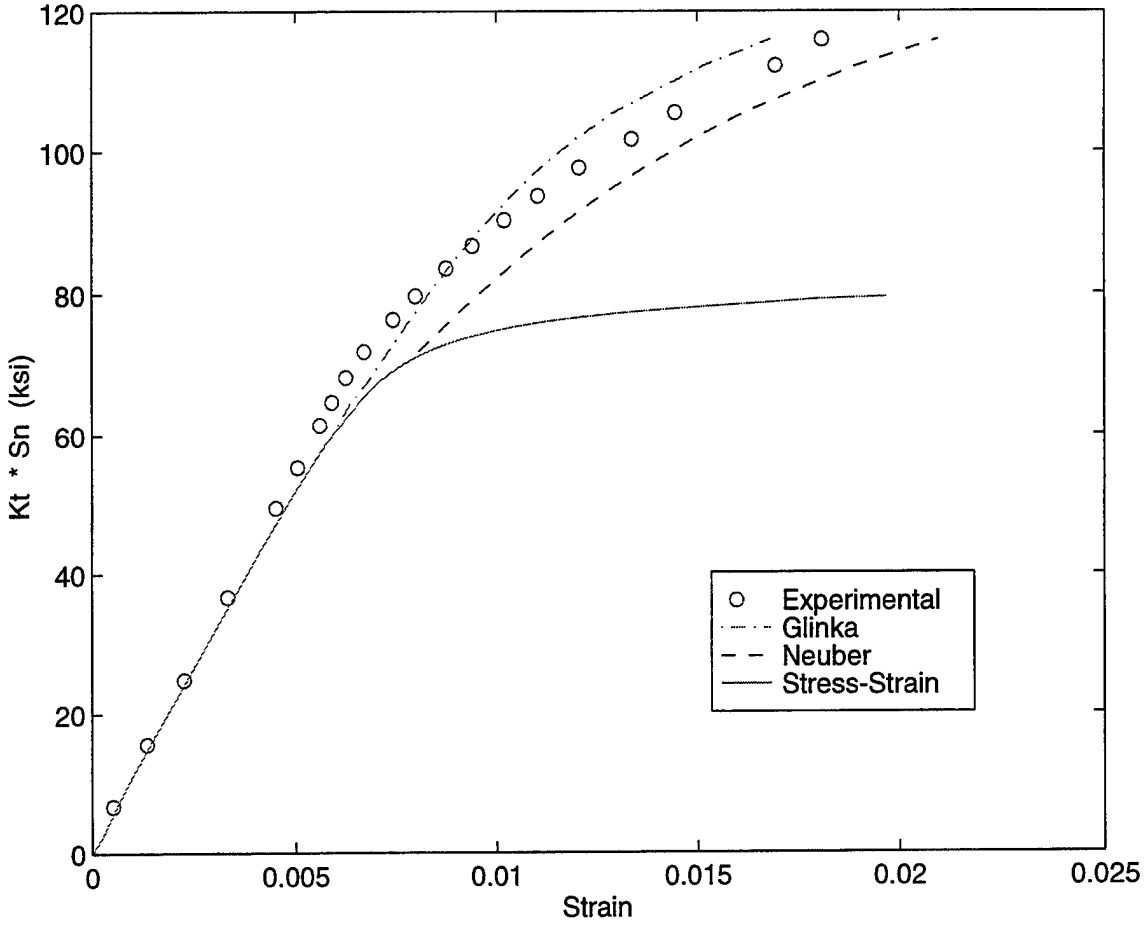

Figure 16. Comparison of Glinka and Neuber Methods for Determining Theoretical Circular Notch Strain in 7075-T6 Aluminum Alloy.

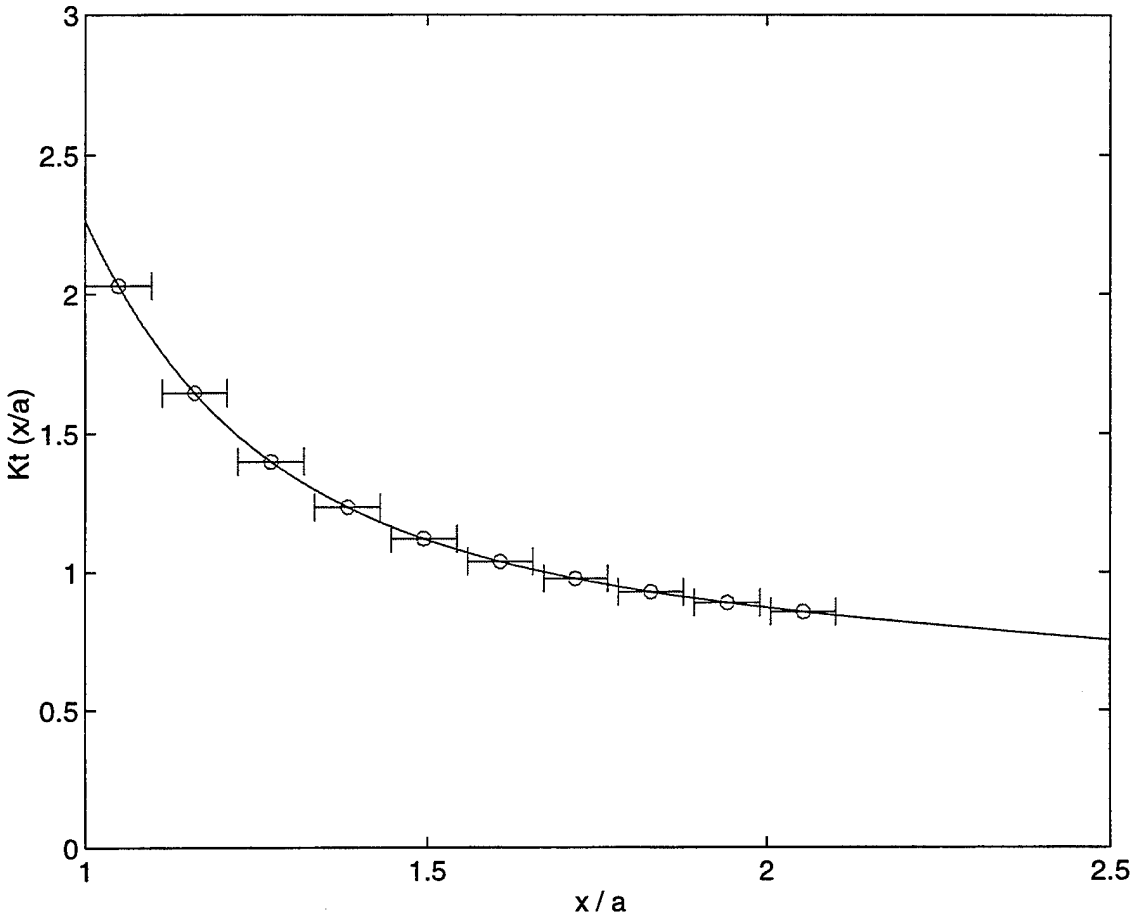

Figure 17. Stress Concentration Factor Gradient Away from the Circular Notch for 7075-T6 Aluminum Alloy. Individual Strain Gage Locations on the 10-Element Strip are Indicated by Horizontal Error Bars.

Superimposed on the gradient curve are the locations of individual strain gages (indicated by horizontal error bars) from the 10-element strip gage. The average stress concentration factor over the strain gage range is indicated by a circle. Next to the hole, K_t = 2.26 using Howland's method. Integrating the gradient over the range of the first strain gage's measuring range to find the average, K_t = 2.04. The stress concentration factor used for the 7075-T6 aluminum tension test results was K_t = 1.90. Although this K_t fell within the range of the first strain gage, it was slightly lower than the average because the first gage was located a small distance away from the edge of the notch.

Figure 18 shows the theoretical strain gradient ahead of the circular notch for two nominal stresses in the elastic range: S_n = 34.0 ksi and S_n = 19.2 ksi. In [10], Glinka's application of the energy-density method resulted in an underestimation of theoretical inelastic strains in strain gradient plots. This study found that theoretical inelastic strains based on Howland's solution were slightly higher than experimental strains. Figure 19 shows strain gradients ahead of the circular notch for several nominal stresses. At low nominal stresses, the gradient is nearly linear. However, as stress is increased, the gradient next to the edge of the notch greatly increases.

2. ARALL 4 Composite

Both Glinka's equation (4.8) and Neuber's equation (4.10), that are used to predict theoretical inelastic stress, depend on the strength coefficient, K,

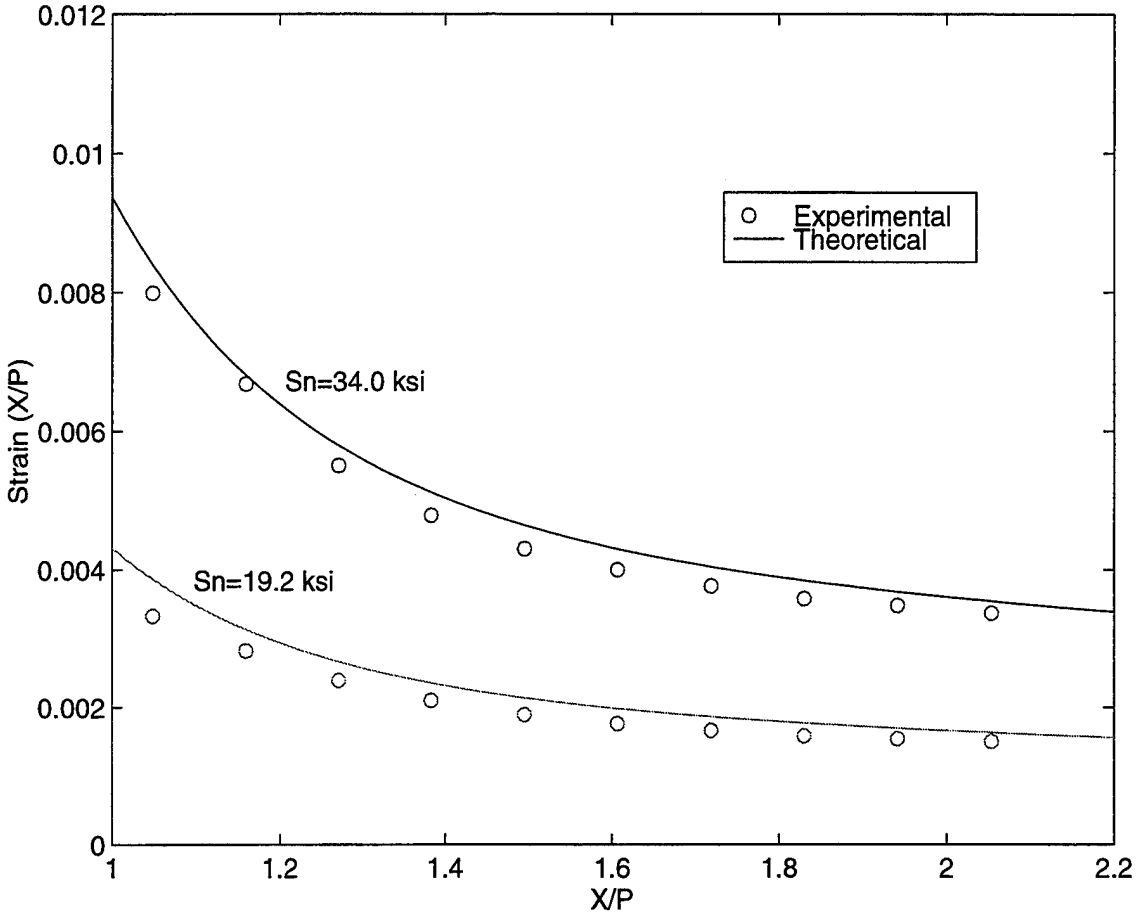

Figure 18. Theoretical and Experimental Elastic Range Strain Gradients Ahead of the Circular Notch in 7075-T6 Aluminum Alloy.

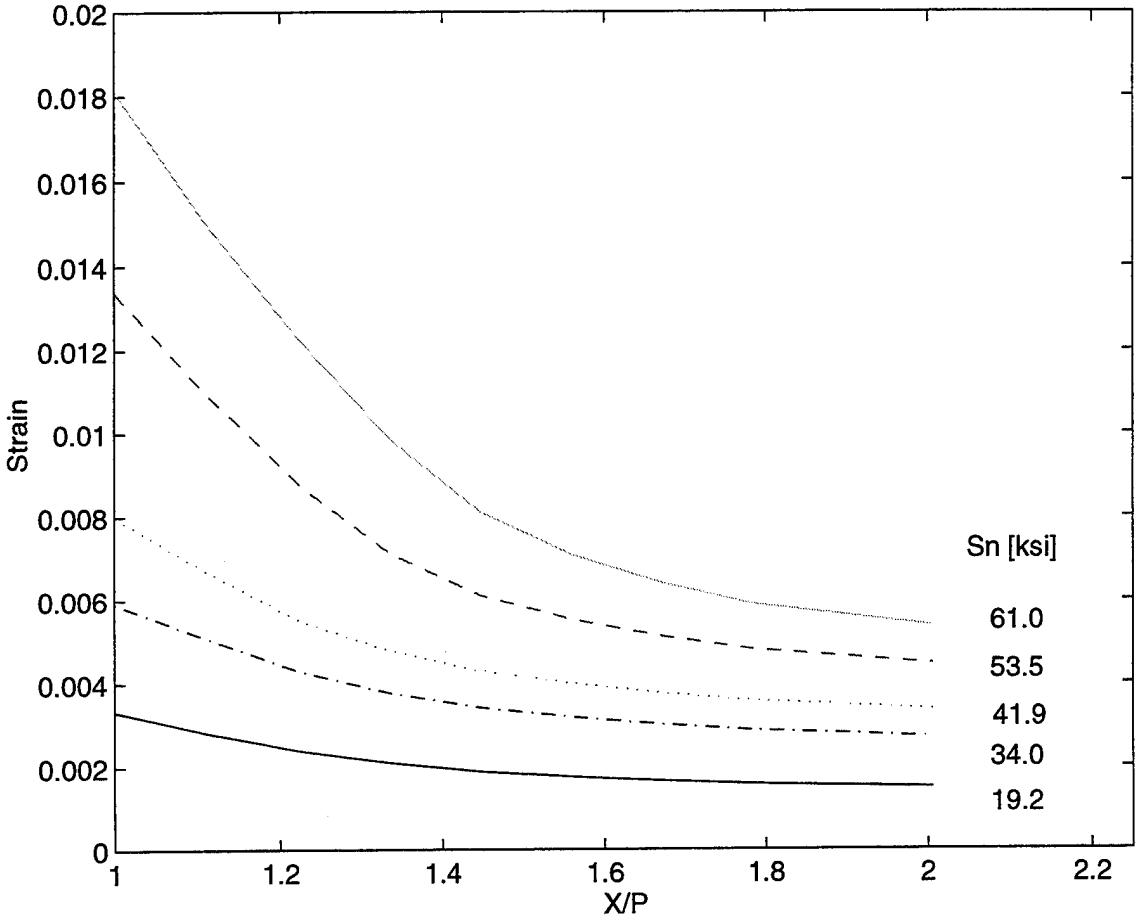

Figure 19. Strain Gradients Ahead of the Circular Notch for Several Nominal Stresses in 7075-T6 Aluminum.

and the strain hardening index, n. Assuming the stress-strain behavior for the ARALL 4 composite can be represented by the Ramberg-Osgood equation (4.1), K and n must be calculated and applied to (4.8) and (4.10). It is evident from Figure 6 that the stress-strain behavior of the ARALL 4 composite is bilinear. Figure 20 shows the plot of log true plastic stress versus log true plastic strain. The method for calculating K and n for the ARALL 4 composite was similar to that for the 7075-T6 aluminum. The straight line in the upper linear region of the curve was used to calculate K = 889 ksi and n = 0.570.

Figure 21 shows the comparison of experimental and theoretical notch strains using Glinka's method. Glinka's method greatly overestimated the inelastic notch strains. Neuber's method was not shown because it produced nearly the same overestimation for inelastic strains that Glinka's method did. Labeled A-B-C is a strain discontinuity for the transition from the linear elastic region to the inelastic region. Inelastic strains were calculated using (4.8). If elastic strains are calculated using Hooke's Law, the jump in strain going from elastic to inelastic behavior is shown as the line A-C. Using (4.7) in the elastic region, the corresponding jump in strain is shown as line B-C. The strain discontinuity between (4.7) and (4.8) can be attributed to the equations' dependence on K and n.

Figure 22 shows the Ramberg-Osgood stress-strain approximation to experimental data for the ARALL 4 composite. Clearly, the Ramberg-Osgood equation does not model bilinear stress-strain behavior. Consequently, the

Glinka equations produced unsatisfactory results. The stress concentration factor used in the ARALL tension test results was 2.10. The sample reached ultimate failure at a tensile load of 8,550 lbs; the corresponding nominal stress was 72.8 ksi.

The strain gradients ahead of the notch for several nominal stresses are shown in Figure 23. The behavior of the gradients as the stress was increased was, as expected, similar to that of the 7075-T6 aluminum.

The prediction for theoretical inelastic notch strains can be greatly improved by using the modified Glinka (4.11) and modified Neuber (4.13) equations. The comparison of the modified Glinka and modified Neuber methods for the ARALL 4 composite in tension is shown in Figure 24. These two new methods give a bound to the experimental data. The overestimation in inelastic strains using the modified Neuber method provides a more conservative approximation. A slight underestimation in notch strains resulted from the modified Glinka method.

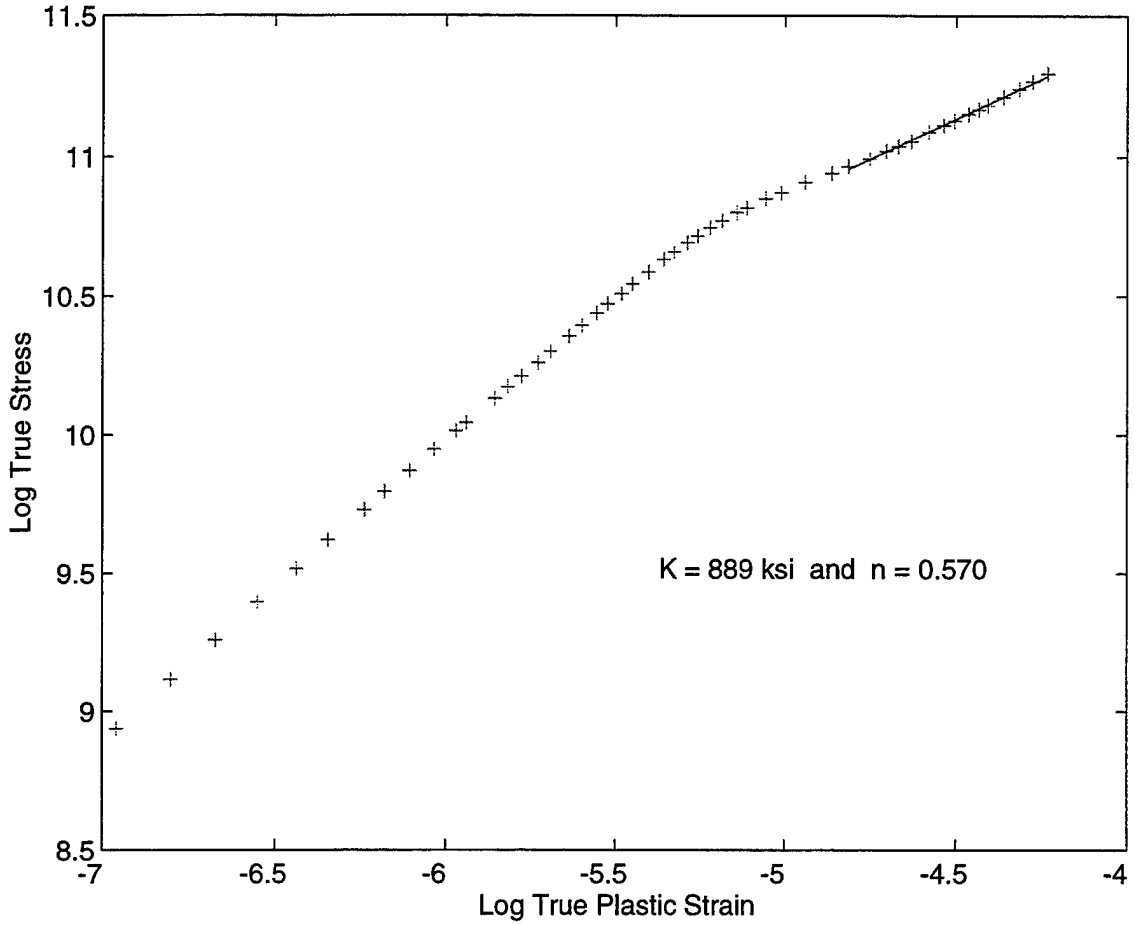

Figure 20. Log of True Plastic Stress-Strain Behavior for ARALL 4 Composite. The Linear Curve Fit Shows where K and n were Determined.

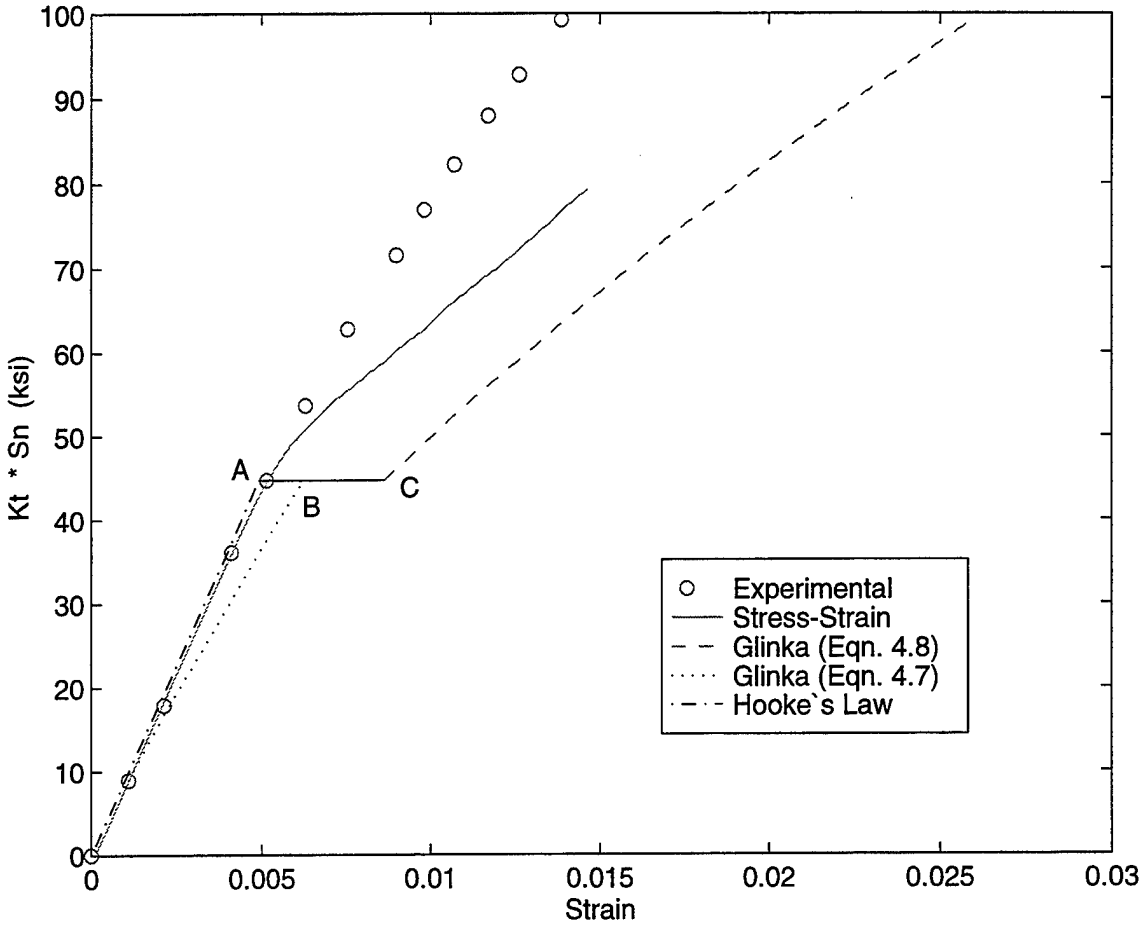

Figure 21. Comparison of Experimental and Theoretical Notch Strains Using Glinka's Method for an ARALL 4 Composite in Tension.

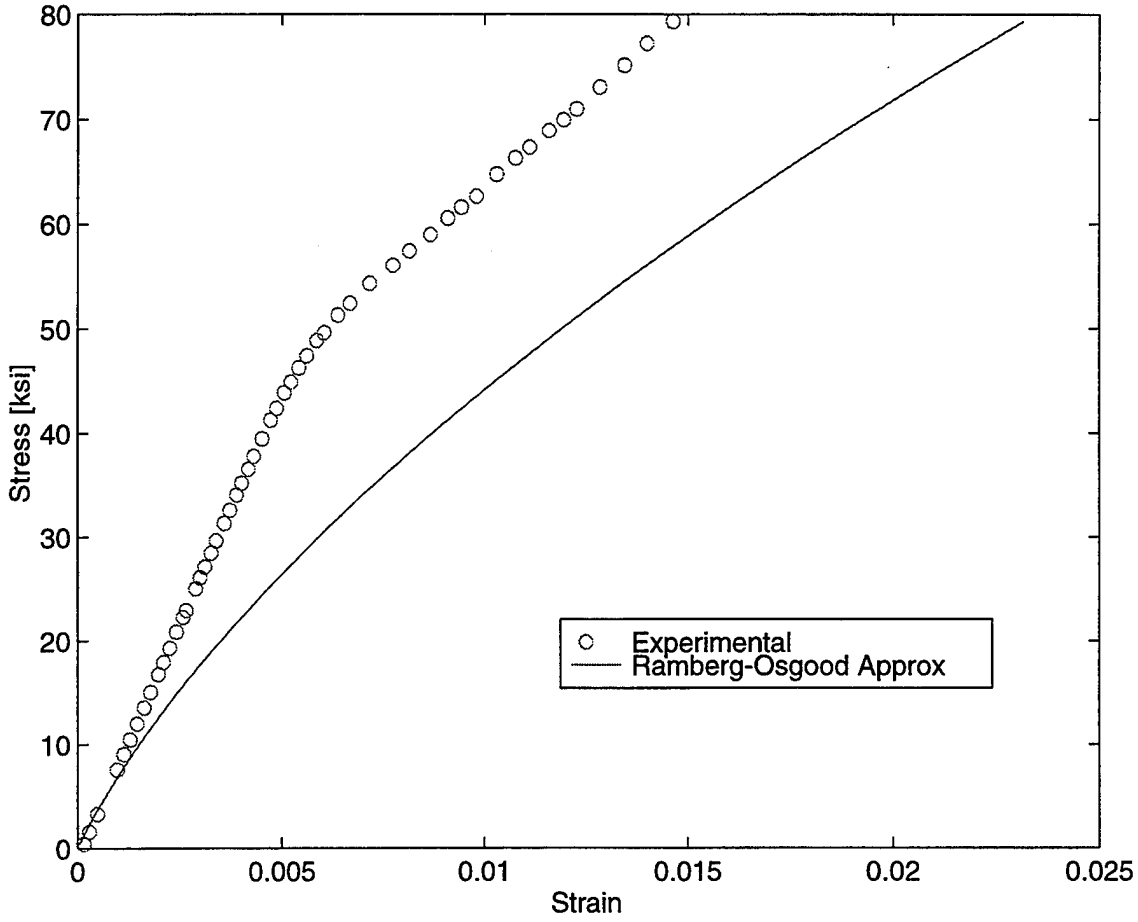

Figure 22. Ramberg-Osgood Stress-Strain Approximation to Experimental Data for ARALL 4 Composite.

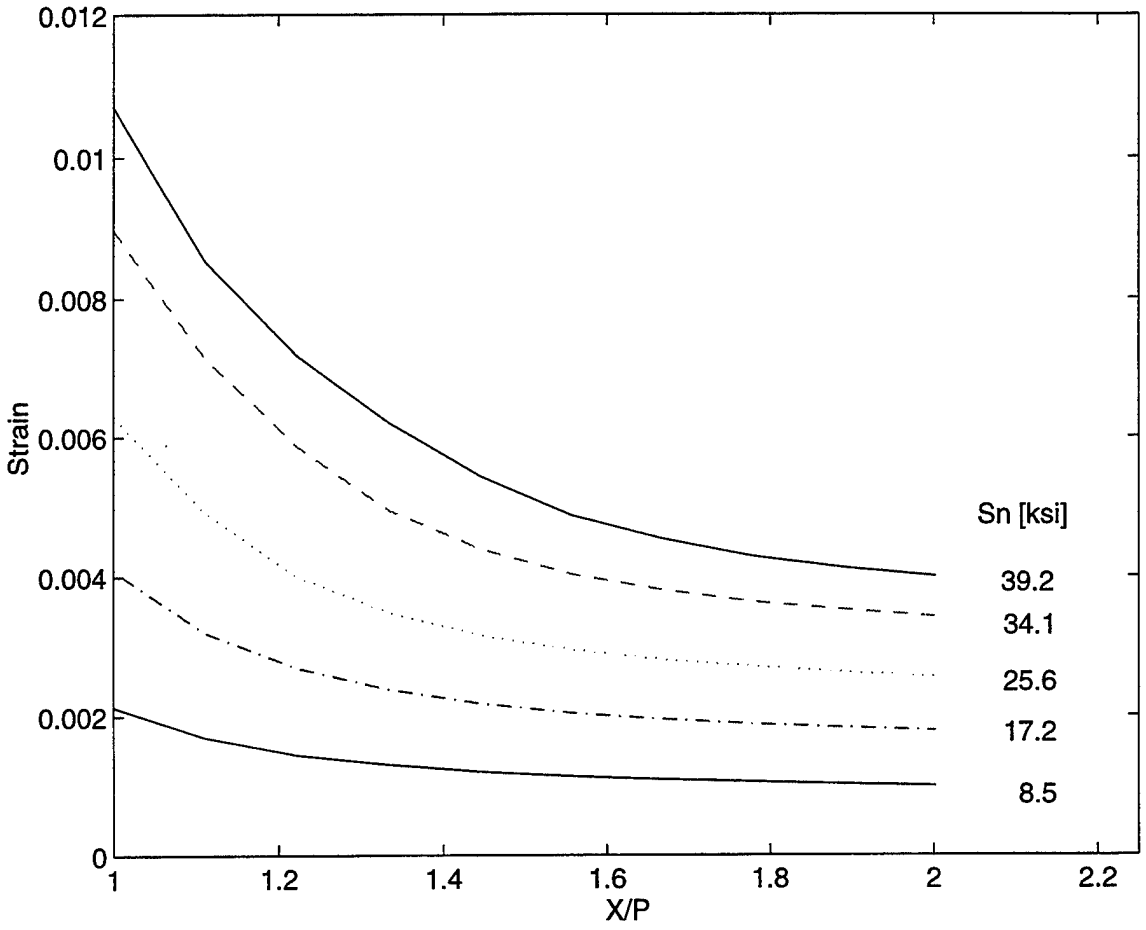

Figure 23. Strain Gradients Ahead of the Circular Notch for Several Nominal Stresses in ARALL 4 Composite.

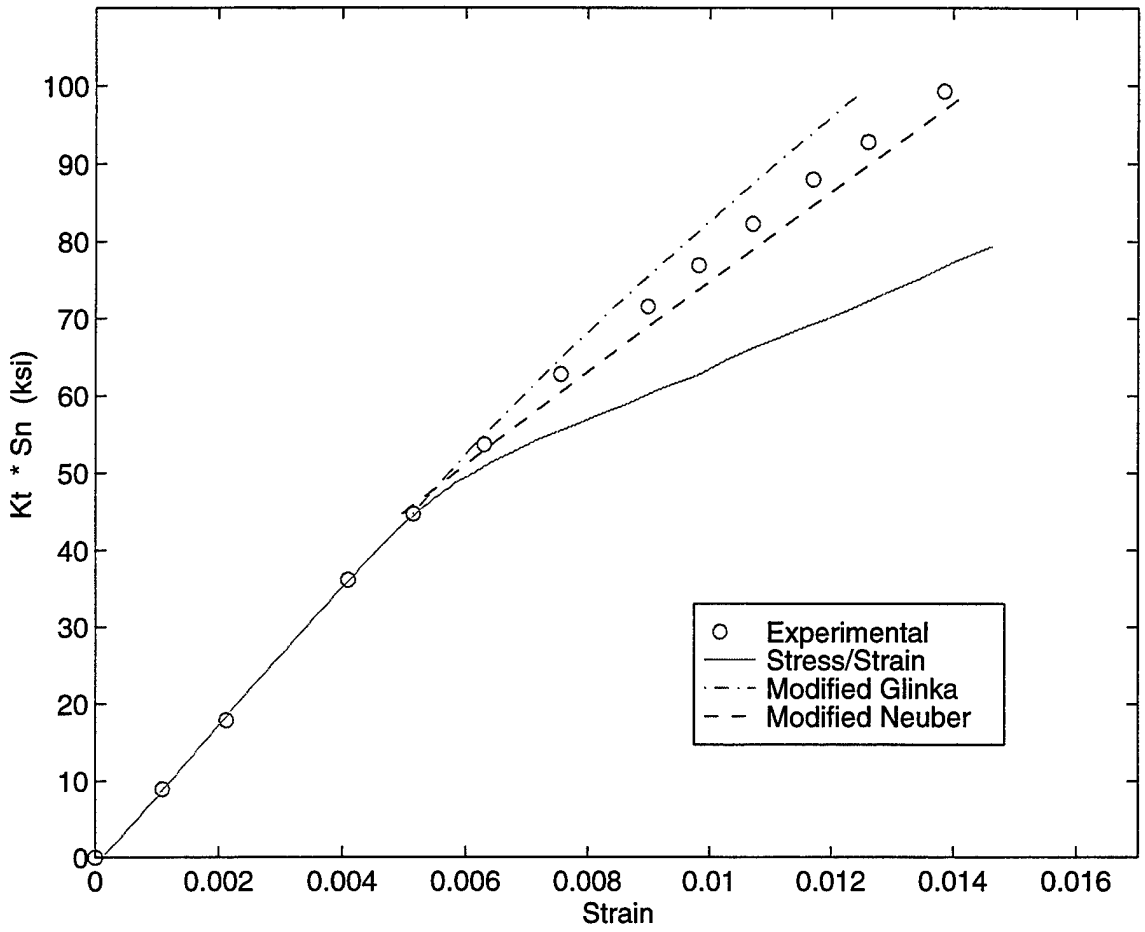

Figure 24. Comparision of Modified Glinka and Modified Neuber Methods for ARALL 4 Composite in Tension.

V. FLEXURAL TEST

Flexural tests were conducted on both 7075-T6 aluminum and ARALL 4 samples. Four-point loading was applied to the quarter points of the samples. This created out-of-plane bending stresses around the circular notch. Flexural testing was conducted to determine whether the Glinka and Neuber relations established for tensile loading could be used predict local inelastic strains for bending. This chapter discusses the experimental apparatus used in conducting the tests, the flexural test procedure, the theory used to determine inelastic bending stresses for both materials, and the test results for the 7075-T6 aluminum and ARALL 4 composite.

A. EXPERIMENTAL APPARATUS

The design of the circular notched samples used in the flexural tests were the same as that used in the tension tests. Sample sizes and dimensions listed in Figure 12 also apply to flexural test samples. The same 10-element strip gages were used but the single back-to-back strain gages were omitted. Also, the Instron test machine used for material property verification was used for flexural tests. However, in order to take incremental load and strain data, the Instron was operated in the manual load control mode. A four-point bend test apparatus was manufactured in accordance with ASTM specifications [30] and the dimensions are shown in Figure 22. The equipment setup is pictured in Figure 23.

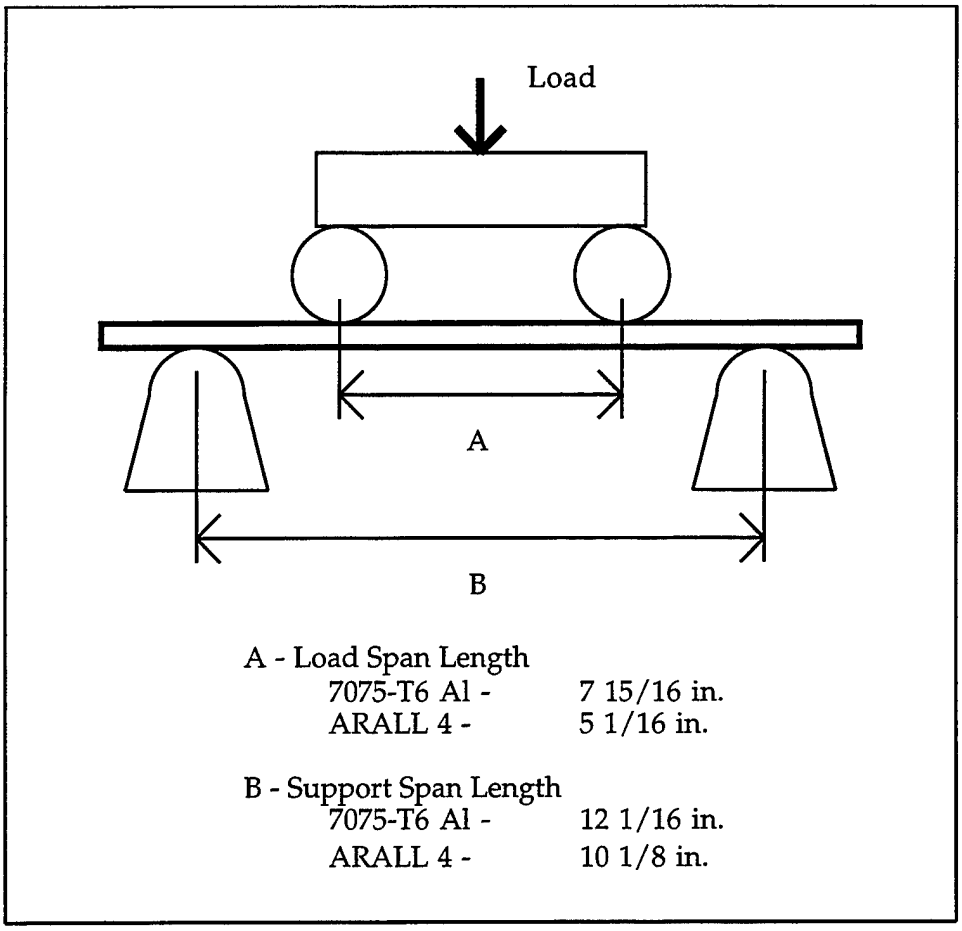

Figure 25. Dimensions of Four-Point Bend Test Apparatus.

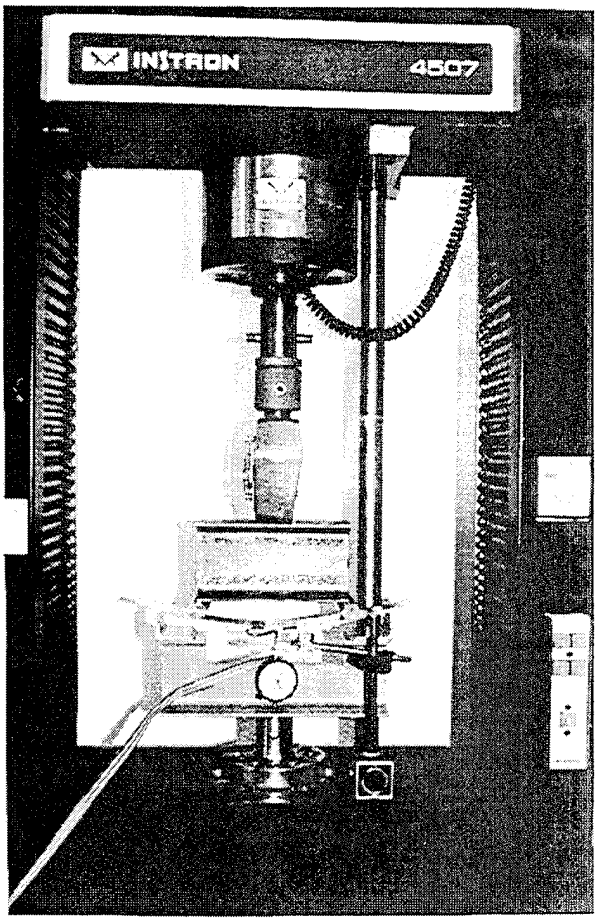

Figure 26. Flexural Test of Circular Notched Sample Subjected to Four-Point Loading.

B. BEND TEST PROCEDURE

A sample was placed on the base of the beam test apparatus and symmetrically aligned. Each strain gage of the 10-element strip gage was zeroed. The top of the beam test apparatus, which weighed 9.6 lbs, was placed on the sample and symmetrically aligned. This condition accounted for the first data point. Incremental loads were then applied to the sample to obtain the remaining data points. For the 7075-T6 aluminum sample, the test was concluded when the sample deflected approx. 2.1 inches, almost touching the base of the beam test apparatus. At this point, the corresponding load was 365 lbs. The maximum load reached before the ARALL 4 sample deflected into the base of the bend test apparatus was 410 lbs. Because the ARALL 4 sample were shorter in length, it could withstand a greater load.

C. THEORY

As tensile loading is increased for a circular notched sample, plastic yielding first occurs at the edge of the notch and progresses away from the notch, towards the edge of the sample. At any location away from the notch, the amount of plastic yielding at that distance will be the same through the sample thickness. Just as in tensile loading, the plastic yielding for bending begins at the edge of the circular notch and progresses outward. However, at a given location away from the notch, as loading is increased plastic yielding begins on the surface of the sample and progresses inward, through the thickness, towards the neutral axis. A small region of plastic yielding is often

referred to as localized plastic yielding. For small localized plastic regions, where nominal bending stress S_n exceeds yield stress σ_Y, the energy density W_{sn} at the notch tip can be calculated based on bending elastic stress.

1. 7075-T6 Aluminum Alloy

The same Glinka relation presented in Chapter IV for localized yielding at the notch tip under tensile loading can be used for bending

$$K_t^2 \frac{S_n^2}{2E} = \frac{\sigma_y^2}{2E} + \frac{\sigma_y}{n+1}\left(\frac{\sigma_y}{K}\right)^{\frac{1}{n}}. \tag{4.7}$$

The Neuber relation for bending is similar to (4.7) but the $\frac{1}{n+1}$ in the second term on the right hand side is replaced with $\frac{1}{2}$, giving

$$K_t^2 \frac{S_n^2}{2E} = \frac{\sigma_N^2}{2E} + \frac{\sigma_N}{2}\left(\frac{\sigma_N}{K}\right)^{\frac{1}{n}}. \tag{5.1}$$

Nominal bending stress is calculated by

$$S_n = \frac{6M}{t^2(D-2d)} \tag{5.2}$$

where M is the bending moment [lbf·in], t is the sample thickness [in.], D is the plate width [in.] and d is the notch diameter [in.].

2. ARALL 4 Composite

The modified Glinka and modified Neuber equations presented in Chapter IV can be also used for bending. The modified Glinka equation is

$$K_t^2 \frac{S_n^2}{2E} = \frac{\sigma_1^2}{2E} + \frac{(\sigma_y^2 - \sigma_1^2)}{2E_t}, \quad \text{for } (\sigma_y < \sigma_1). \tag{4.11}$$

The modified Neuber equation is

$$K_t^2 \frac{S_n^2}{2E} = \frac{\sigma_N}{2}\left(\frac{\sigma_N - \sigma_1}{E_t} + \frac{\sigma_1}{E}\right). \tag{4.13}$$

D. RESULTS

1. 7075-T6 Aluminum Alloy

Figure 27 shows the comparison of Glinka and Neuber methods for determining theoretical inelastic notch strain in out-of-plane bending. The Glinka approximation was much closer to the experimental strains than the Neuber approximation. For low and moderate local inelastic strains, the Glinka method was an overestimation but in the high yield region, the Glinka method tended to underestimate the local inelastic strain.

Figure 28 shows the load versus deflection curve for 7075-T6 aluminum in out-of-plane bending. The tangent to the linear region of the curve was shown to identify the departure from linearity. Figure 29 shows several strain gradients ahead of the circular notch. These gradients are slightly different when compared to those for the 7075-T6 aluminum samples in tension loading. The slope of the gradient next to the notch was lower for bending than tension. As in the tension test, the strain gradients in bending approached a constant value away from the notch.

The stress concentration factor used in Figures 27 and 29 was 1.20.

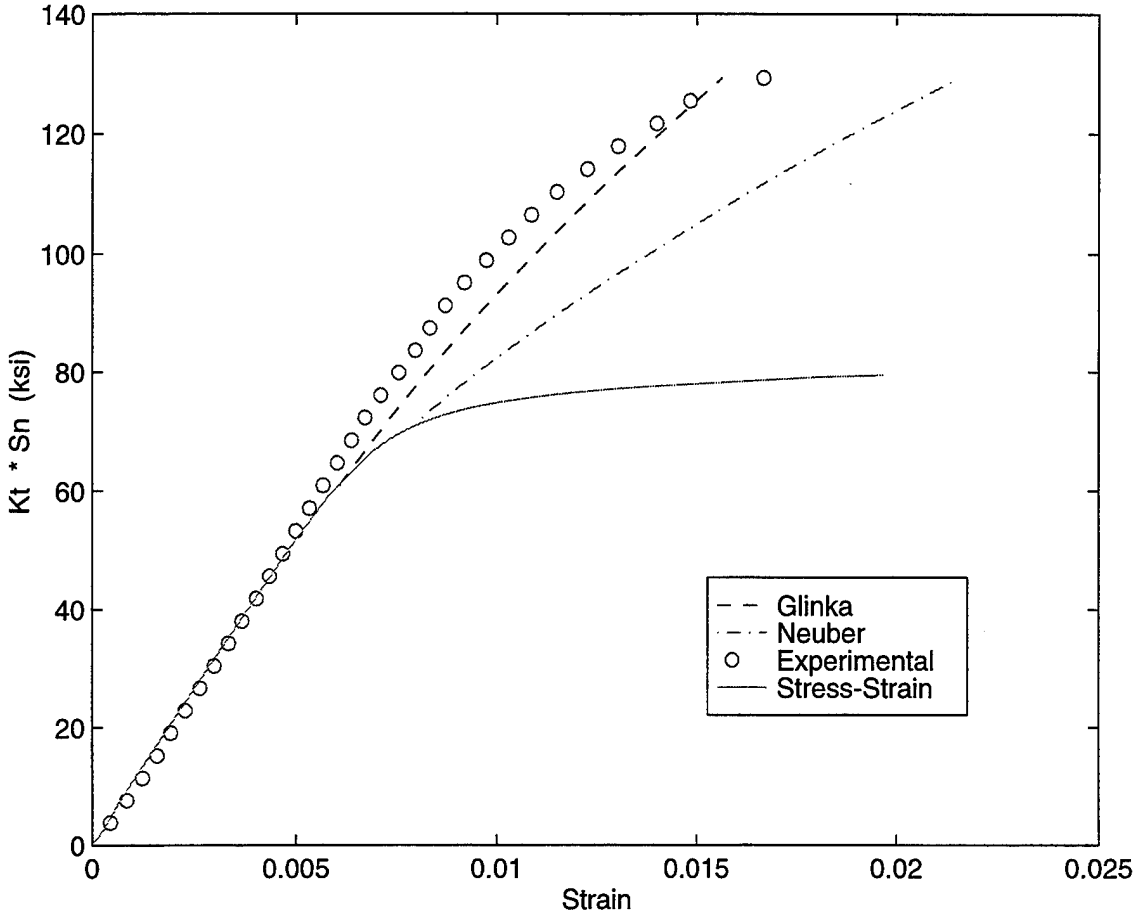

Figure 27. Comparison of Glinka and Neuber Methods for Determining Theoretical and Experimental Circular Notch Strain for 7075-T6 Aluminum in Out-of-Phase Bending.

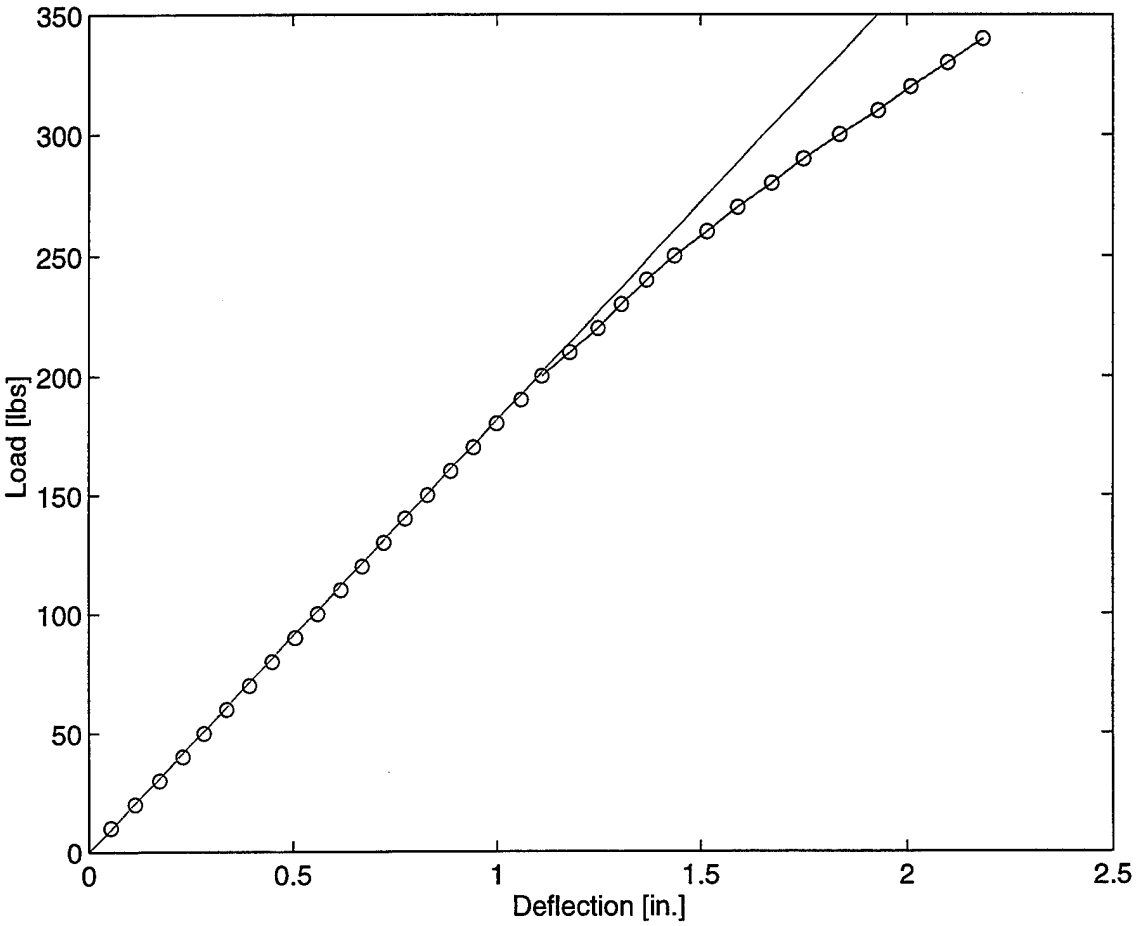

Figure 28. Load-Deflection Curve for 7075-T6 Aluminum in Out-of-Plane Bending.

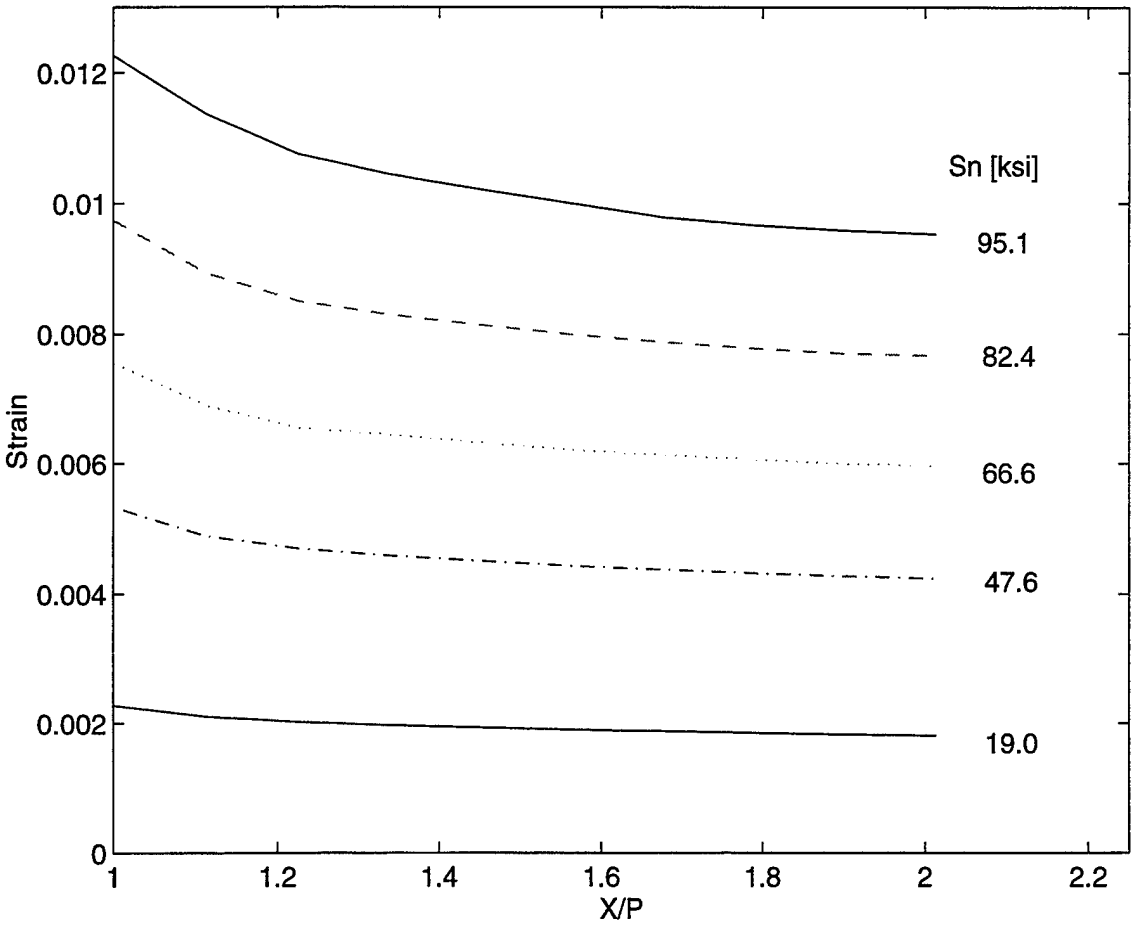

Figure 29. Strain Gradient Ahead of the Circular Notch for Several Nominal Stresses for 7075-T6 Aluminum in Out-of-Plane Bending.

Peterson has plotted several curves for stress concentration factors subject to transverse bending of a finite-width plate with a circular hole [35]. The experimental circular notch diameter (a) to sample width (W) ratio was 0.34. Peterson plotted the stress concentration factor curves for $\frac{a}{W}$ from 0 to 0.2. If the appropriate curve is extrapolated to $\frac{a}{W} = 0.34$, the resulting stress concentration factor next to the notch is approximately 1.40. As discussed in Chapter IV, the strain gage was located small distance from the edge of the notch. The strain gage averaged the stress concentration factor gradient over the gage's measured area. The 15 percent difference in experimental and theoretical stress concentration factors can also be attributed to a slight off-centering of the circular notch by 0.03 in. (0.76 mm) during the machining process.

2. ARALL 4 Composite

Figure 30 shows the comparison of Glinka and Neuber methods for determining theoretical and experimental circular notch strain for ARALL 4 composite in out-of-plane bending. Glinka's equation (4.7) was used within the elastic-plastic region to predict theoretical notch strains. This was justified by Glinka's statement in Reference 10, "... within some range of the nominal bending stress $S_n > \sigma_Y$, only localized plastic yielding can occur in the analyzed section, whereas under tensile loading plastic yielding of the whole section would occur." The discontinuity line A-B shows the transition from elastic

strains calculated using Hooke's Law and inelastic strains calculated using Neuber's method. Although the Glinka method achieved a closer approximation, both methods greatly overestimated local inelastic strains. At low inelastic yielding, the two methods predicted a strain response that exceeded the material stress-strain diagram. As in Chapter IV, the equations' dependence on the strength coefficient (K) and strain hardening index (n) from the Ramberg-Osgood relation resulted in unsatisfactory results.

Figure 31 shows the comparison of the modified Glinka and the modified Neuber methods for out-of-plane bending. These methods greatly improved the inelastic strain approximation as compared to Figure 30. Both modified methods underestimated experimental notch strain at large plastic deformations. For small plastic deformations, the modified Neuber method was a slightly conservative approximation.

In Figure 32, the load-deflection curve for the ARALL 4 composite in out-of-plane bending is shown. Figure 33 shows several strain gradients ahead of the circular notch for the ARALL 4 composite in out-of-plane bending. The stress concentration factor used in the ARALL 4 tests was 1.05.

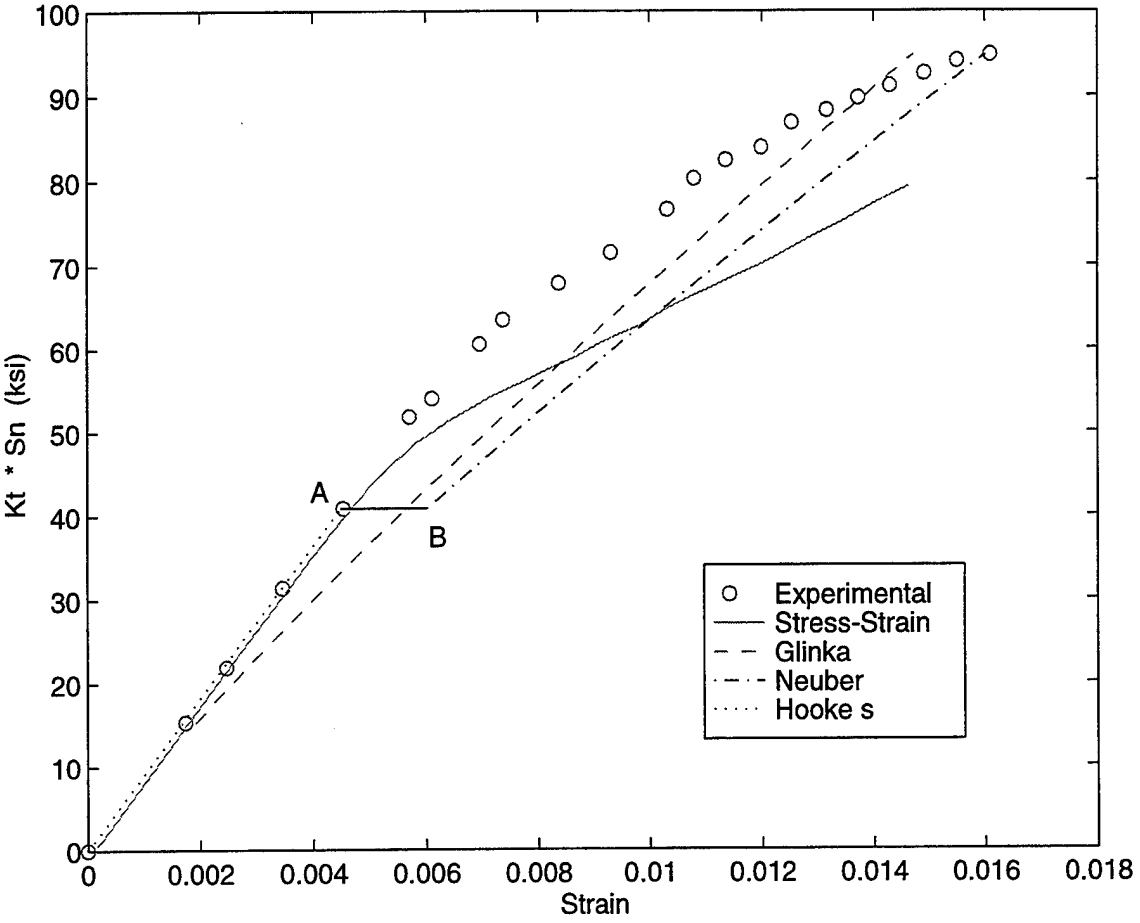

Figure 30. Comparison of Glinka and Neuber Methods for Determining Theoretical and Experimental Notch Strain for ARALL 4 Composite in Out-of-Plane Bending.

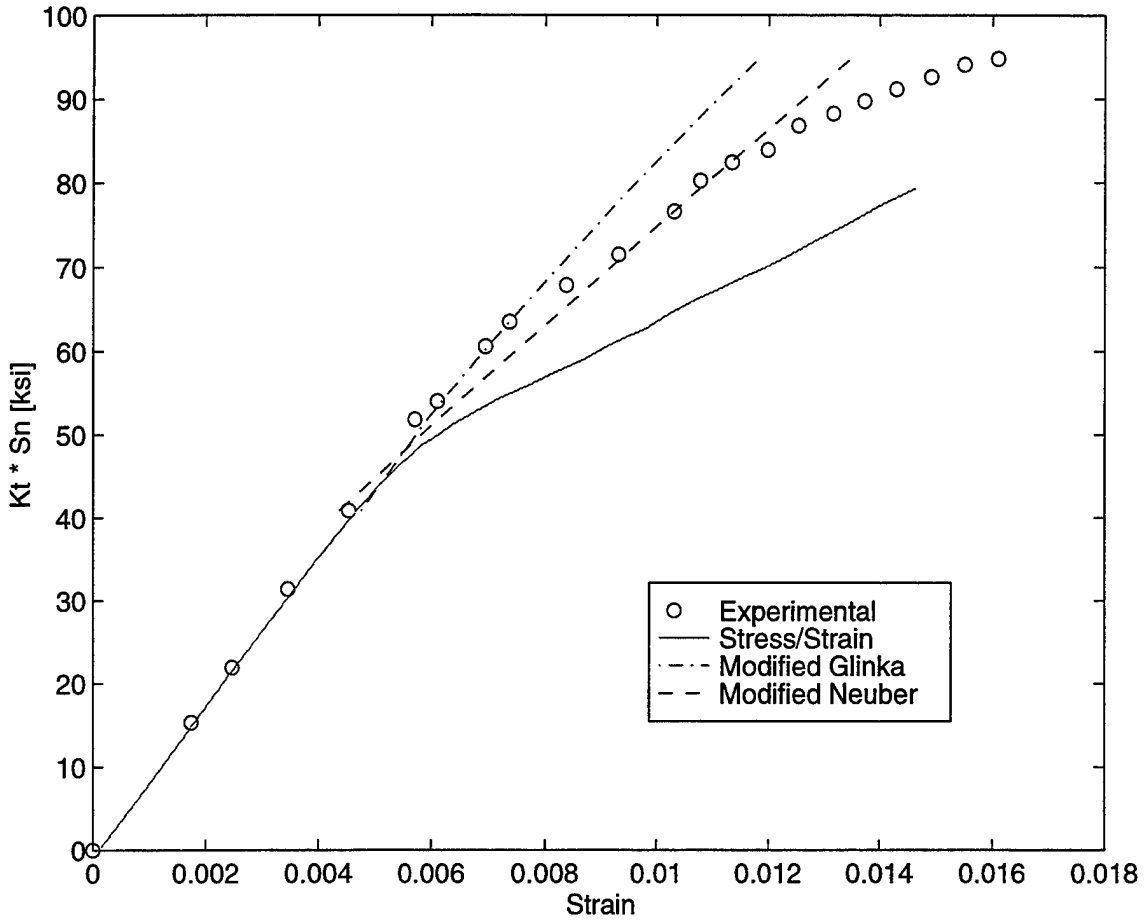

Figure 31. Comparison of Modified Glinka and Modified Neuber Methods for ARALL 4 Composite in Out-of-Plane Bending.

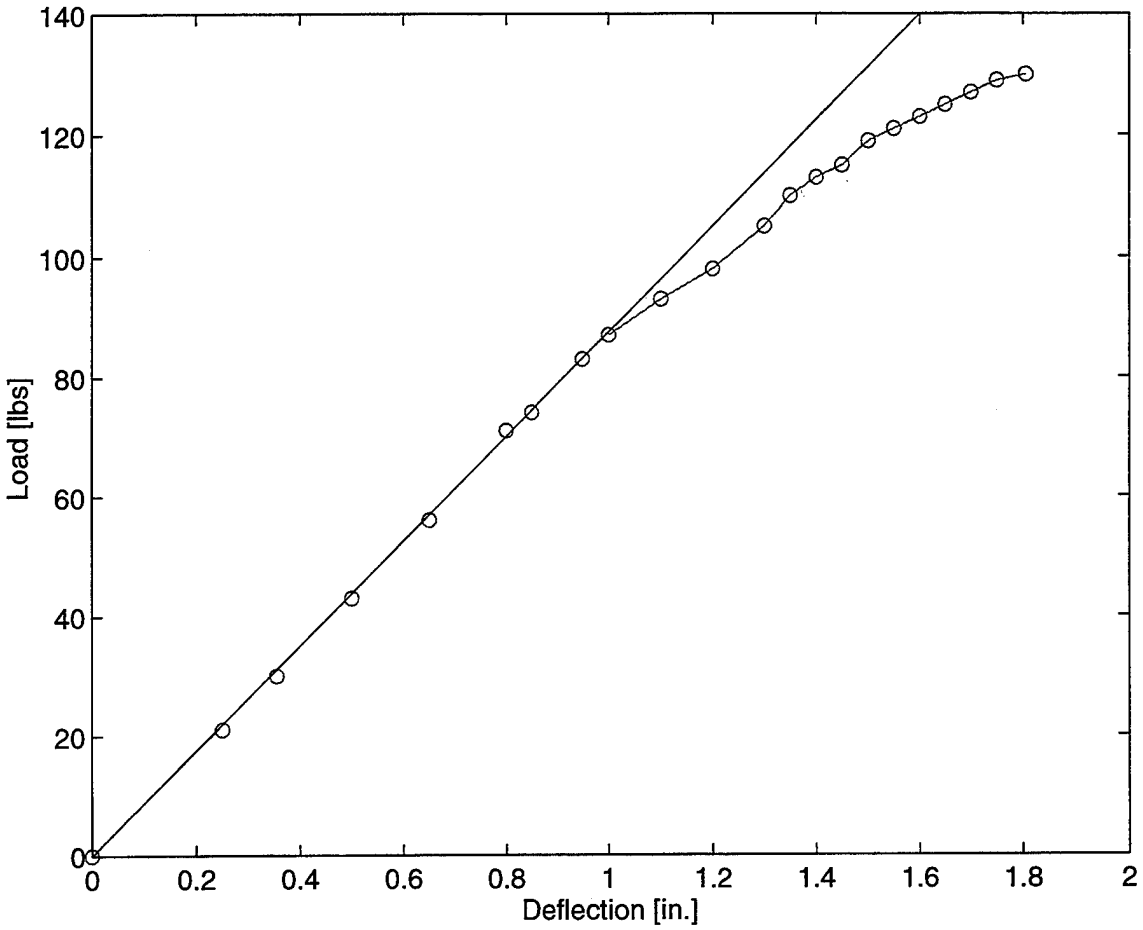

Figure 32. Load-Deflection Curve for ARALL 4 Composite in Out-of-Plane Bending.

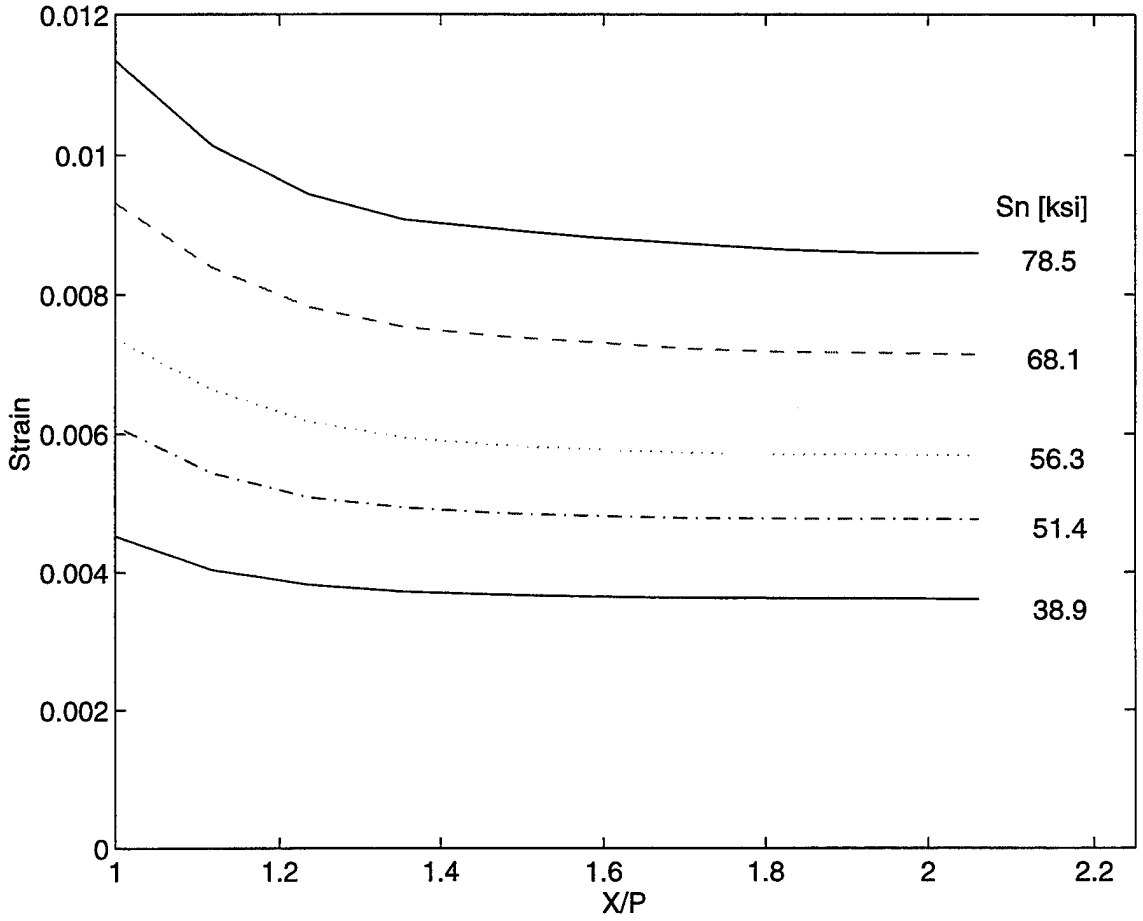

Figure 33. Strain Gradient Ahead of the Circular Notch for Several Nominal Stresses for ARALL 4 Composite in Out-of-Plane Bending.

VI. CONCLUSIONS AND RECOMMENDATIONS

Because the behavior of inelastic stresses/strains around a circular notch is complex, an accurate solution has not been found. Approximate methods have been proposed that provide reasonable results. Specific findings of this study include:

- Neuber's method always predicted inelastic circular notch strains that were larger than those using Glinka's method.

- As expected, Glinka's method of approximating theoretical inelastic notch strain produced good results for the 7075-T6 aluminum in tension. Theoretical inelastic strains were within 15 percent of the experimental data.

- The Glinka method provided good theoretical strain predictions for a 7075-T6 aluminum alloy subjected to out-of-plane bending.

- Both the Glinka and Neuber methods demonstrated unsatisfactory results when applied to an ARALL 4 composite subjected to tension and out-of-plane bending. Because separate equations were used to predict strains in the elastic and inelastic region, a strain discontinuity was created in the transition from linear elastic to inelastic behavior. ARALL 4 has a bilinear

stress-strain curve and Glinka's and Neuber's method are based on the Ramberg-Osgood relation. This relation does not represent the composite's bilinear stress-strain behavior well.

- The modified Glinka and modified Neuber methods produced good results for predicting theoretical inelastic notch strains in an ARALL 4 composite subjected to out-of-plane bending.

- For an ARALL 4 composite in tension, the modified Glinka and modified Neuber methods can be used to bound experimental notch strains. Using the standard Glinka and Neuber methods, bounding of experimental notch strains was also observed for the 7075-T6 aluminum sample in tension.

- Theoretical notch strain predictions for samples in tension were better than samples in out-of-plane bending. This was true for the standard and modified Glinka and Neuber methods.

- Previous studies found Neuber's method produced conservative predictions for theoretical inelastic notch strains. For the ARALL 4 composite in out-of-plane bending, the modified Neuber method predicted inelastic notch strains that were non-conservative.

Future research in the inelastic stress distribution around notches should consider the following recommendations:

- Due to the large stress concentration factor gradient next to a circular notch, a precise stress concentration factor at the notch tip is difficult to obtain. Precision could be improved by using larger sample widths and notch diameters with small strain gages. However, the problems associated with increased sample lengths and grip configuration at the ends for tension tests requires careful planning. To record large inelastic strains, the strain gage grid must be as large as possible to avoid internal gage failure. The trade off is that strain gages tend to average the strain over the area covered by the grid. For a nonuniform strain distribution, the reported strain measurement will less than the maximum strain. Consequently, the precise determination of the stress concentration factor at the notch tip will be more difficult.

- Instead of using strain gages, Moiré interferometry could be used to measure the local displacement/strain more accurately.

- A finite element analysis could be conducted. FEA would provide highly accurate results and incorporate a degree of flexibility. Different sample and notch geometries could be modeled for different sample loadings.

LIST OF REFERENCES

1. Howland, R. C. J., "On the Stresses in the Neighbourhood of a Circular Hole in a Strip Under Tension," *Philosophical Transactions of the Royal Society of London*, Series A229, 1930, pp. 49-86.

2. Dumont, C., "Stress Concentration Around an Open Circular Hole in a Plate Subjected to Bending Normal to the Plane of the Plate," National Advisory Committee of Aeronautics, Technical Note 740, 1939.

3. Hill, R., "On Discontinuous Plastic States with Special Reference to Localized Necking in Thin Sheets," *Journal of the Mechanics and Physics of Solids*, Vol. 1, 1952, pp. 19-30.

4. Peterson, R. E., *Stress Concentration Factors*, John Wiley and Sons, 1974.

5. Prasad, C. B. And Shuart, M. J., "Moment Distributions Around Holes in Symmetric Composite Laminates Subjected to Bending Moments," *AIAA Journal*, Vol. 28, No. 5, May 1990, pp. 877-882.

6. Neuber, H., "Theory of Stress Concentraion for Shear-Strained Prismatic Bodies with Arbitrary Nonlinear Stress-Strain Law," ASME *Journal of Applied Mechanics*, Vol. 28, No. 4, 1961, pp. 544-551.

7. Theocaris, P. S. and Marketos, E., "Elastic-Plastic Analysis of Perforated Thin Strips of Strain-Hardening Material," *Journal of the Mechanics and Physics of Solids*, Vol. 12, 1964, pp. 377-390.

8. Hutchinson, J. W., "Singular Behaviour at the End of a Tensile Crack in a Hardening Material," *Journal of the Mechanics and Physics of Solids*, Vol. 16, 1968, pp. 13-31.

9. Molski,K. and Glinka, G., "A Method of Elastic-Plastic Stress and Strain Calculation at a Notch Root," *Material Science Engineering*, Vol. 50, 1981, pp. 93-100.

10. Glinka, G., "Energy Density Approach to Calculation of Inelastic Strain-Stress Near Notches and Cracks," *Engineering Fracture Mechanics*, Vol. 22, No. 3, 1985, pp. 485-508.

11. Glinka, G., "Calculation of Inelastic Notch-Tip Strain-Stress Histories Under Cyclic Loading," *Engineering Fracture Mechanics*, Vol. 22, No. 5, 1985,

pp. 839-854.

12. Hoffman, M. and Seeger, T., "A Generalized Method for Estimating Multiaxial Elastic-Plastic Notch Stresses and Strains, Part 1: Theory," ASME *Journal of Engineering Materials and Technology*, Vol. 107, No. 4, Oct. 1985, pp. 250-254.

13. Glinka, G., Ott, W. and Nowack, H., "Elastoplastic Plane Stress Analysis of Stresses and Strains at the Notch Root," ASME *Journal of Engineering Materials and Technology*, Vol. 110, July 1988, pp. 195-204.

14. Sharpe, W., Yang, C., and Tregoning, R., "An Evaluation of the Neuber and Glinka Relations for Monotomic Loading," ASME *Journal of Applied Mechanics*, Vol. 59, Oct. 1992, pp. S50-S56.

15. Lee, Y., Chang, Y., and Wong, H., "A Constitutive Model for Estimating Multiaxial Notch Strains," ASME *Journal of Engineering Materials and Technology*, Vol. 117, No. 1, Jan. 1995, pp. 33-40.

16. ASTM E8-95a: "Standard Test Methods for Tension Testing of Metallic Materials, " American Society for Testing of Materials, ASTM Standards, 1995.

17. ASTM E111-82: "Standard Test Method for Young's Modulus, Tangent Modulus, and Chord Modulus," American Society for Testing of Materials, ASTM Standards, 1988.

18. ASTM E132-86: "Standard Test Method for Poisson's Ratio at Room Temperature ," American Society for Testing of Materials, ASTM Standards, 1992.

19. American Society for Metals, *Metals Handbook*, ASM International, Vol. 2, Table 108, 1985, pp. 115-117.

20. American Society for Metals, *Metals Handbook*, ASM International, Vol. 2, 1985, p. 116.

21. ASTM E111-82: "Standard Test Method for Young's Modulus, Tangent Modulus, and Chord Modulus," American Society for Testing of Materials, ASTM Standards, 1988, p. 224.

22. ASTM E132-86: "Standard Test Method for Poisson's Ratio at Room Temperature," American Society for Testing of Materials, ASTM Standards, 1992.

23. ASTM E111-82: "Standard Test Method for Young's Modulus, Tangent Modulus, and Chord Modulus," American Society for Testing of Materials, ASTM Standards, 1988.

24. National Advisory Committee of Aeronautics, Technical Note 902, "Description of Stress-Strain Curves by Three Parameters," by Ramberg, W., and Osgood, W.R., 1943.

25. Bannantine, J., Comer, J., and Handrock J., *Fundamentals of Metal Fatigue Analysis*, Prentice Hall, 1990, p. 45.

26. American Society for Metals,*Tensile Testing*, ASM International, 1992, p. 15.

27. McClintock, F.A., "Stastical Estimation: Linear Regression and the Single Variable," *Research Memo 274, Fatigue and Plasticity Laboratory*, Cambridge: Massachusettes Institute of Technology, Feb. 1987.

28. Beckwith, T., Marangoni, R., and Lienhard V, *Mechanical Measurements*, Addison-Wesley, 1993.

29. ASTM D3039-95: "Standard Test Method for Tensile Properties of Polymer Matrix Composite Materials," American Society for Testing of Materials, ASTM Standards, 1995.

30. ASTM D790-92: "Standard Test Methods for Flexural Properties of Unreinforced and Reinforced Plastics and Electrical Insulating Materials," American Society for Testing of Materials, ASTM Standards, 1992.

31. American Society for Metals, *Metals Handbook*, ASM International, Vol. 2, 1985, p. 70.

32. Chawla, K.K., *Composite Materials: Science and Engineering*, Springer-Verlag, Table 2.5, 1987, p. 37.

33. American Society for Metals,*Tensile Testing*, ASM International, 1992, p. 192.

34. ASTM D790-92: "Standard Test Methods for Flexural Properties of Unreinforced and Reinforced Plastics and Electrical Insulating Materials," American Society for Testing of Materials, ASTM Standards, 1992, p. 158.

35. Peterson, R. E., *Stress Concentration Factors*, John Wiley and Sons, Fig. 160, 1974, p. 231.

INITIAL DISTRIBUTION LIST

No. Copies

1. Defense Technical Information Center.....2
   8725 John J. Kingman Rd., STE 0944
   Fort Belvoir, Virginia 22060-6218

2. Dudley Knox Library.....2
   Naval Postgraduate School
   Monterey, California 93943-5101

3. Chairman, Code ME.....1
   Department of Mechanical Engineering
   Naval Postgraduate School
   Monterey, California 93943-5000

4. Professor Young W. Kwon, Code ME/Kw.....2
   Department of Mechanical Engineering
   Naval Postgraduate School
   Monterey, California 93943-5100

5. Professor Gerald H. Lindsey, Code AA/Li.....1
   Department of Aeronautics and Astronautics
   Naval Postgraduate School
   Monterey, California 93943-5100

6 Naval Engineering Curricular Office, Code 34.....1
   Naval Postgraduate School
   Monterey, California 93943-5100

7. LT Kenneth S. Long 2
   304 Sweetgum
   League City, Texas 77573